INTERNATIONAL JOURNAL OF CLIMATOLOGY
Int. J. Climatol. (2016)
Published online in Wiley Online Library
(wileyonlinelibrary.com) DOI: 10.1002/joc.4874

RMetS
Royal Meteorological Society

A 60-year reconstructed high-resolution local meteorological data set in Central Sahel (1950–2009): evaluation, analysis and application to land surface modelling

C. Leauthaud,[a†]* B. Cappelaere,[a] J. Demarty,[a] F. Guichard,[b] C. Velluet,[a] L. Kergoat,[c] T. Vischel,[d] M. Grippa,[c] M. Mouhaimouni,[e] I. Bouzou Moussa,[f] I. Mainassara[g,a] and B. Sultan[h]

[a] *HydroSciences Montpellier (HSM), CNRS, IRD, Université de Montpellier, Montpellier, France*
[b] *Centre National de Recherches Météorologiques (CNRM), UMR 3589, CNRS, Météo-France, Toulouse, France*
[c] *Géosciences Environnement Toulouse (GET), CNRS, IRD, Université de Toulouse, Toulouse, France*
[d] *Laboratoire des Transferts en Hydrologie et Environnement, UMR 5564, CNRS, IRD, Université Grenoble I, France*
[e] *Service Analyses Climatologiques, Direction de la Météorologie Nationale du Niger, Niamey, Niger*
[f] *Département de géographie, Université Abdou Moumouni, Niamey, Niger*
[g] *Représentation au Niger, IRD, Niamey, Niger*
[h] *Sorbonne Universités (UPMC Paris 6)-CNRS-IRD-MNHN, LOCEAN/IPSL, IRD, Paris, France*

ABSTRACT: The Sahel has experienced strong climate variability in the past decades. Understanding its implications for natural and cultivated ecosystems is pivotal in a context of high population growth and mainly agriculture-based livelihoods. However, efforts to model processes at the land–atmosphere interface are hindered, particularly when the multi-decadal timescale is targeted, as climatic data are scarce, largely incomplete and often unreliable.

This study presents the generation of a long-term, high-temporal resolution, multivariate local climatic data set for Niamey, Central Sahel. The continuous series spans the period 1950–2009 at a 30-min timescale and includes ground station-based meteorological variables (precipitation, air temperature, relative and specific humidity, air pressure, wind speed, downwelling long- and short-wave radiation) as well as process-modelled surface fluxes (upwelling long- and short-wave radiation, latent, sensible and soil heat fluxes and surface temperature). A combination of complementary techniques (linear/spline regressions, a multivariate analogue method, artificial neural networks and recursive gap filling) was used to reconstruct missing meteorological data. The complete surface energy budget was then obtained for two dominant land cover types, fallow bush and millet, by applying the meteorological forcing data set to a finely field-calibrated land surface model. Uncertainty in reconstructed data was expressed by means of a stochastic ensemble of plausible historical time series.

Climatological statistics were computed at sub-daily to decadal timescales and compared with local, regional and global data sets such as CRU and ERA-Interim. The reconstructed precipitation statistics, ∼1 °C increase in mean annual temperature from 1950 to 2009, and mean diurnal and annual cycles for all variables were in good agreement with previous studies. The new data set, denoted NAD (Niamey Airport-derived set) and publicly available, can be used to investigate the water and energy cycles in Central Sahel, while the methodology can be applied to reconstruct series at other stations.

KEY WORDS Niamey airport station; ERA-40; ERA-Interim; CRU; fallow savannah; millet; gap filling; synoptic data

Received 1 June 2015; Revised 22 July 2016; Accepted 28 July 2016

1. Introduction

The African Sahel is one of the regions in the world that has experienced the strongest climatic variations in the past decades (Hulme, 1992, 2001; Nicholson, 2001). In Central Sahel, annual precipitation underwent a strong decrease in the 1970s–1980s followed by a partial recovery in the 1990s–2000s compared with the period 1950–1969 (Le Barbe *et al*., 2002; Lebel and Ali, 2009), while extreme rainfall occurrence could be increasing (Panthou *et al*., 2014). In parallel, the annual temperature rose faster than the global average, with an increase in mean above 1 °C during March–October from 1950 to 2000 (Guichard *et al.*, 2015). Together with important vegetation and land use change (Séguis *et al.*, 2004; Leblanc *et al.*, 2008; Hiernaux *et al.*, 2009a, 2009b; Dardel *et al.*, 2014), and in a context of high population growth and rainfed subsistence farming, these climate variations have strong implications for food and water resources (e.g. Mahé and Olivry, 1999; Favreau *et al.*, 2009) that call for a better understanding of underlying physical processes. In particular, surface–atmosphere interactions are critical factors for the Sahelian water and energy cycles and influence vegetation characteristics (Moorcroft, 2003), groundwater recharge (Massuel *et al.*, 2011; Ibrahim *et al.*, 2014) and atmosphere dynamics (Xue *et al.*, 2010). Estimations of

* Correspondence to: C. Leauthaud, HSM, 300 avenue Emile Jeanbrau, 34000 Montpellier, France. E-mail: crystele.leauthaud@cirad.fr

†Present address: CIRAD, UMR G-EAU, F-34398 Montpellier, France.

the surface water and energy budgets do exist for short periods (e.g. Kahan *et al.*, 2006; Saux-Picart *et al.*, 2009; Velluet *et al.*, 2014), but estimations of long-term fluctuations are still lacking as climatic data are scarce, largely incomplete and sometimes unreliable.

Hydro-meteorological data are a valuable asset to investigate process dynamics at the land–atmosphere interface. Many reliable meteorological – observational or analysis – data sets have long been available for various time/space resolutions and coverage in other regions of the world (e.g. Klok and Klein Tank, 2009; Herrera *et al.*, 2012; Chimani *et al.*, 2013). Research in the Sahel, especially concerning the water and energy cycles, has been impeded by the limited amount of observational data and the lack of consistent and homogeneous climate databases, with relevant space–time resolutions and appropriate extensions in space/time (coverage, period, missing data) to study the water and energy cycles.

For instance, rainfall variability in the Sahel is characterized by the intermittency and convective properties of rainfall. These properties directly influence the variability of many other meteorological variables (radiation, temperature, etc.) and the interaction with the surface (e.g. run-off). Modelling of the water and energy balance requires high-temporal resolutions as the convective peaks of rain cells can only be captured at a 30-min or less time step. Hence, gridded data sets (e.g. CRU, Mitchell and Jones, 2005) developed on a monthly basis with a typical resolution of 100 km are not suitable for fine-scale hydrological studies. In addition, available high-temporal resolution data sets (ERA-40, Uppala *et al.*, 2005; ERA-Interim, Dee *et al.*, 2011) do not yet provide reliable estimates of precipitation for this region (e.g. Meynadier *et al.*, 2010).

Concerning extension in space and time, the few long-term data sets from institutional ground stations, with low network density and substantial missing data, are of limited use for many applications, at least directly. Recently, some high space–time resolution ground (e.g. the AMMA-CATCH network, Lebel *et al.*, 2009) or remotely sensed data sets (Nicholson *et al.*, 2003; Gosset *et al.*, 2013) have been made available, but provide limited historical depth. When it comes to land surface response variables, no multi-decadal field-based series exist, even at a local scale.

Making the best use of scarce data also raises methodological issues that are far from being fully resolved. Many gap-filling procedures exist. For instance, methods routinely applied to eddy-covariance flux data have been discussed in detail (Falge *et al.*, 2001; Moffat *et al.*, 2007). In comparison, gap filling of meteorological data has been discussed to a lesser degree, although it is often required for climatological analysis, modelling studies or model/data comparisons (e.g. Schwalm *et al.*, 2010). Applicability and use of gap-filling methods in the Sahel region still need to be assessed, especially for long-term data sets.

A direct consequence of these issues is that modelling efforts regarding the land–atmosphere interface are hampered as soon as the multi-decadal timescale is targeted. Putting the emphasis on the time-wise description (long time-range with high-temporal resolution) that is key for surface process studies in the Sahel, rather than on resolving for spatial variability, the objectives of this research were threefold:

- to produce a continuous and consistent series of the main variables required in land surface-type models, for the location of Niamey, which is typical of the Central Sahel climate, at a 30-min time step over the period 1950–2009. These meteorological variables were: precipitation, air temperature, relative and specific humidity, surface pressure, wind speed, downwelling long- and short-wave radiation. Special care was taken to ensure inter-variable coherence of these variables and to estimate uncertainty in the determination of missing data;
- to apply this meteorological series to a field-based land surface model, in order to provide for the same period a reference simulated series of the main land surface response fluxes for two major land cover types, namely millet crop and fallow bush. Estimated variables at a 30-min time step included latent and sensible heat fluxes, upwelling long- and short-wave radiation and surface temperature;
- to analyse the main properties of these series and compare them with those of pre-existing data sets.

The complete new data set is referred to as the Niamey Airport-derived (NAD) data set and is comprised of the NAD-M meteorological series and of the simulated NAD-S land surface response series. The paper is organized into five sections. The original data, general approach and data set construction and application are described in Section 2. Section 3 analyses the main characteristics of the new data set, in terms of extent of reconstructed data and of scale-dependent properties (uncertainty, climatology, relation to available local and gridded series) at diurnal to decadal timescales. The value of the NAD data set is discussed in Section 4 and conclusions are drawn in Section 5. Appendices S1 and S2 (Supporting information) and Appendix A1 provide technical details on methodology and skill of reconstruction steps, respectively. Note that all Figures but 3 and 7 are in colour in the online paper version.

2. Methodology of NAD construction and application

2.1. Naming conventions

The variables of interest in this study consist of meteorological variables and of land surface response variables. These variables are referred to via symbols, which are all specified in Table 1. Table 1 also defines the acronyms of the various data sets that are considered in this study.

Table 1. List of variables and data sets. Characteristics of gridded data sets are provided in Appendix A2.

Code		Meaning
Variables		
G, H, LE		Soil heat, sensible and latent flux, respectively ($W\,m^{-2}$)
LW, $SW_{down, up, net}$		Long- and short-wave downwelling, upwelling and net radiation ($W\,m^{-2}$)
P		Precipitation (mm)
Pa		Air pressure (hPa)
q		Specific humidity ($g\,kg^{-1}$)
R_{ext}		Extraterrestrial radiation ($W\,m^{-2}$)
RH		Relative humidity (%)
Ta, Ts		Air and soil temperature (°C)
U		Wind speed ($m\,s^{-1}$)
Subscripts		
24 h, 12 h, 3 h, 30 min, 5 min		24-hour, 12-hour, 3-hour and 5-minute cumulated precipitation. $P_{12\,h}$ precipitation occurs from 6 AM to 6 PM and from 6 PM to 6 AM
mean, max, min		Daily mean, maximum and minimum (for Ta, RH)
Data sets for the Niamey airport station		
DLY1, DLY2, DLY3, DLY4	Original (see Table 2)	Daily (24 h) or twice daily (12 h) data for 1950–1980, 1981–2003, 1950–1990 and 1950–2003, respectively
FVE1, FVE2	Original (see Table 2)	Instantaneous (5 min) precipitation data for 1956–1998 and 1990–2009, respectively
SYN1, SYN2, SYN3	Original (see Table 2)	Synoptic (3 h) data for 1950–1980, 1979–1995, 1996–2009, respectively
NAD	Final	Niamey Airport-Derived data set, produced by this study
NAD-M	Final	Meteorological data component of NAD
NAD-S	Final	Land surface characteristics component of NAD, for fallow bush (NAD-Sf) and millet (NAD-Sm) land cover types
Other data sets (observations, gridded data, meteorological re-analyses)		
ARM		Atmospheric Radiation Measurement Climate Research Facility
BEST		Berkeley Earth Temperature Averages for 1950-2009
CRU		Climatic Research Unit TS3.1 for 1950-2009
ERA-40		European Centre for Medium-Range Weather Forecasts (ECMWF) re-analysis for 1958-2001
ERA-Interim		ECMWF re-analysis for 1979-2009
GISS		Goddard Institute for Space Studies land surface temperatures for 1950-2009
GHCN		Global Historical Climatology Network version 2 and the Climate Anomaly Monitoring System global land surface temperatures for 1950-2009
MERRA		Modern-Era Retrospective analysis for Research and Applications for 1979-2009
NCEP2		National Centers for Environmental Prediction - Department of Energy Atmospheric Model Intercomparison Project II (NCEP–DOE AMIP-II) Reanalysis for 1979-2009
SRB		Surface Radiation Budget for 1984–2007

2.2. Available data

Long-term climatic series are scarce in Central Sahel. The Niamey airport station (2.166°E, 13.483°N, 222 m, Figure 1) data stand as an exception with rare 5-min precipitation observations beginning as early as 1956, as well as valuable long-term daily and synoptic data. However, these various data were found in sparse form from different sources, as nine different data sets (Table 2; see Figure 2 for a display of data availability). Four sets (DLY1, DLY2, DLY3 and DLY4) provided 24 h/12 h values for P, Ta and/or RH over different and sometimes redundant periods. Few data were missing in these four sets until 1980, after which only RH_{mean} and $P_{24\,h}$ were available (Figure 2). Three synoptic series (SYN1, SYN2, SYN3) provided 3-h observations of Ta, RH, Pa and U, albeit some large gaps. Finally, two sets (FVE1 and FVE2) provided 5-min precipitation data, $P_{5\,min}$, covering over 85% of observed rainy days (Figure 2(i) and (j)). Taken all together, these data sets provided a rare picture of the climate over the period 1950–2009: although missing data were unavoidable at the 3-h or 5-min time steps, daily scale information covered most days over this period.

In addition, four independent, shorter but quality checked data sets from nearby stations (Figure 1 and Table 3) were used as ancillary data sets. The Wankama data set (Wankama-South site of AMMA-CATCH observatory, Cappelaere *et al*., 2009; Ramier *et al*., 2009) and the Atmospheric Radiation Measurement data set (ARM, Slingo *et al*., 2006; Miller and Slingo, 2007) provided high time resolution data for P, Ta, RH, Pa, U, LW_{down} and SW_{down}. They were used to calibrate and/or validate the methods used to produce NAD. The Banizoumbou (Goutorbe *et al.*, 1994) and Agrhymet data sets, which provided Ta, RH and SW_{down}, were used for general comparison purposes.

2.3. General approach

To produce a gap-free, homogeneous and uncertainty-bounded data series, a multi-step screening and gap-filling methodology was devised, allowing to account for the

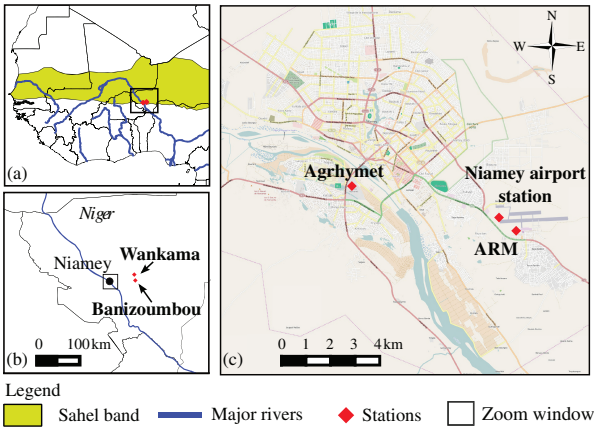

Figure 1. Location of Niamey airport and ancillary stations in nested-scale boxes: (a) West Africa, (b) South-West of Republic of Niger, (c) City of Niamey (openstreetmap base map).

variety of situations that originated from such different factors as variable types, interdependencies, or duration and resolution of available data. Specifically, the meteorological data set (NAD-M) was produced in four successive steps, and it was in turn used to estimate land surface fluxes (NAD-S) with a physics-based soil–vegetation–atmosphere transfer (SVAT) model (Table 4).

The first step consisted in quality checking all available Niamey airport meteorological data sets and grouping sets with equal time steps. The second step gap-filled the 3-h and 5-min meteorological series. Depending on missing data characteristics, methods ranged from simple spline and linear regressions for variables with strong temporal or inter-variable correlations, to more complex methods jointly estimating multiple variables at the same time step. In the third step, all meteorological series were transformed to a 30-min time step. This time step appeared as the best compromise between a good temporal resolution and uncertainty in downscaling the synoptic data, as well as being well-suited to modelling the water and energy cycles in this environment. In the fourth step, radiative fluxes SW_{down} and LW_{down}, which were not measured at Niamey airport station but are frequently required, were estimated using artificial neural networks. The fifth and final step produced the land surface variables for fallow bush and millet land cover types, with a SVAT model.

An ensemble approach was used to characterize the uncertainty related to the gap-filling and estimation methods of NAD-M. Each gap-filling operation, devised with a stochastic component, was repeated 100 times. Altogether, these ensemble members reflect a range of possible values for the missing data, and form the complete data set of meteorological data (NAD-M). To reduce computation time, the NAD-S series of land surface response variables was constructed as a subset of ten ensemble members, through random selection from the NAD-M ensemble. Note that only this subset was used for the analysis of resulting uncertainties in the various NAD variables, as discussed in Section 3.

The following sections further describe these successive steps, while detailed technical aspects are provided in Appendices S1 and S2.

2.4. Step I: quality checking and standardization of original data sets

The hydro-meteorological data for Niamey airport presented three major drawbacks: they (1) came from different sources, in separate files and various formats, possibly including alternative sensors; (2) were incomplete over the period 1950–2009 and (3) with different time steps.

Special care was therefore taken to check their coherence. Easily detectable errors were corrected, through despiking and direct inconsistency removal (characteristics of detected errors are supplied in Appendix A3). Data were then assembled into four distinct series, consisting,

Table 2. Raw data sets initially available at the Niamey airport station. Measurement height for climatic variables was 2m, except for U (10 m). Ta_{mean} and RH_{mean} were calculated from their daily maximum and minimum values. 'AMMA' means that data were obtained at http://database.amma-international.org. Websites to access data are specified in Appendix S3.

Data set	Versions	Period[a]	Variables	Temporal resolution	References
DLY1	WMO[b] (AMMA)	1950–1980	$P_{24\,h}$, RH_{max}, Ta_{max}, RH_{min}, Ta_{mean} $P_{12\,h}$	24 h 12 h	–
DLY2	SIEREM[c]	1981–2003	RH_{mean}	24 h	Boyer *et al.*, 2006
DLY3	SIEREM	1950–1990	$P_{24\,h}$	24 h	Boyer *et al.*, 2006
DLY4	DMN[d] (AMMA)	1950–2003	$P_{24\,h}$	24 h	Le Barbe *et al.*, 2002; Panthou *et al.*, 2014
SYN1	WMO (AMMA)	1950–1980[e]	Ta, RH, Pa, U	3 h	–
SYN2	WMO (AMMA)	1979–1995	Ta, U	3 h	–
SYN3	WMO (AMMA)	1996–2009	Ta, RH, Pa, U	3 h	–
FVE1[f]	DMN	1956–1998	$P_{5\,min}$	5 min	Lubès-Niel *et al.*, 2001
FVE2	AMMA-CATCH	1990–2009	$P_{5\,min}$	5 min	Balme *et al.*, 2006

[a]For synoptic data: first and last year for which all data available.
[b]World Meteorological Organization.
[c]Système d'Informations Environnementales sur les Ressources en Eau et leur Modélisation.
[d]Direction de la Météorologie Nationale.
[e]End date for Pa: 1965.
[f]Event data.

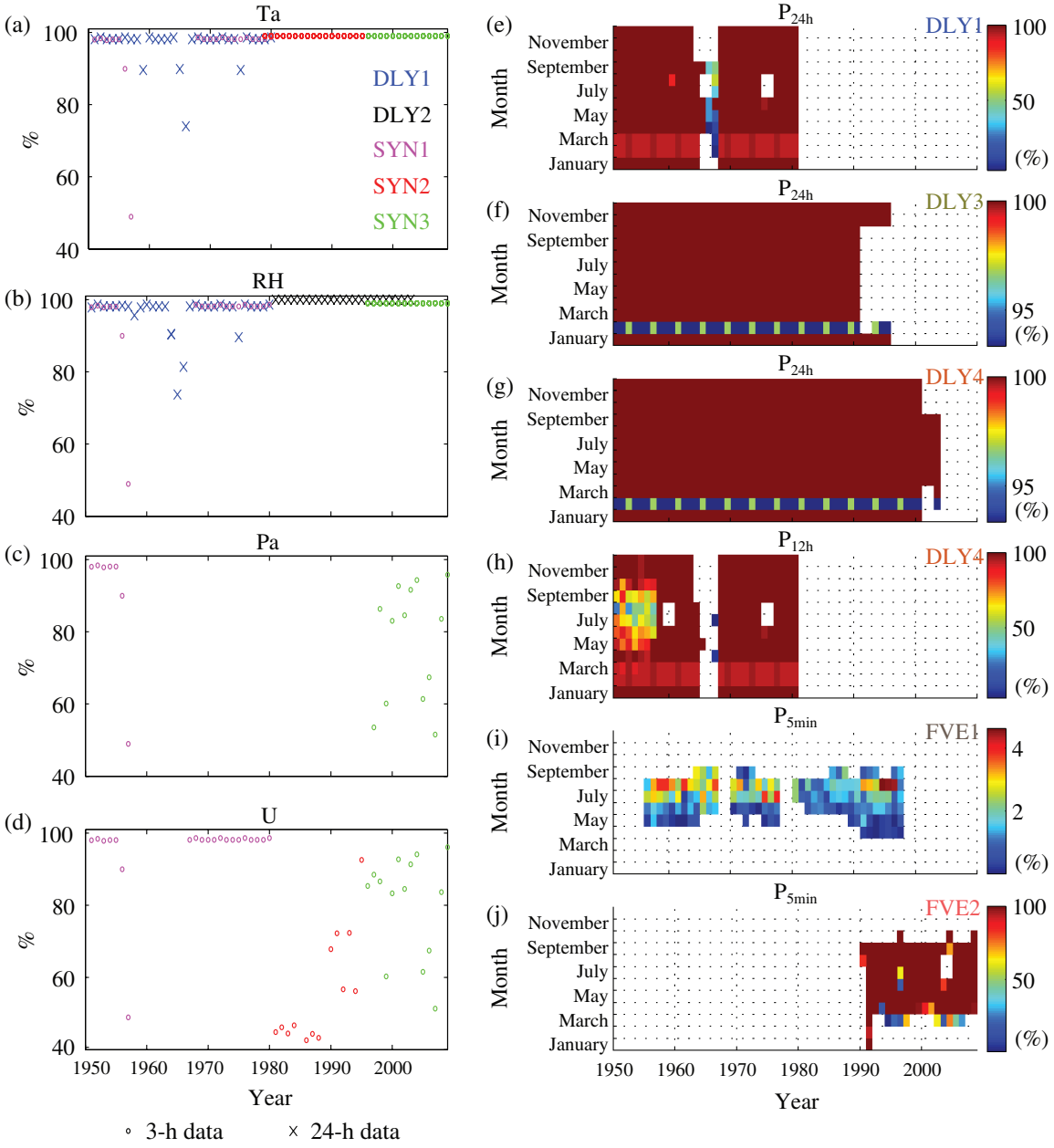

Figure 2. Data availability over time. Left: Yearly percentage of available data for Ta, RH, Pa and U (top to bottom) for the raw series (colour code in (a) and symbol code on bottom line. Right: Percentages of available data for P ($P_{24\,h}$, $P_{12\,h}$ and $P_{5\,min}$, top to bottom) mapped by year and month, for raw series.

respectively, of 24-h ($P_{24\,h}$, Ta_{mean} and RH_{mean}), 12-h ($P_{12\,h}$), 3-h synoptic (Ta, RH, Pa, and U) and 5-min ($P_{5\,min}$) resolution data. As our objective was to produce high-temporal resolution data, the 3-h and 5-min series were selected as the base series, while the 24-h and 12-h series were kept to provide additional information for the gap-filling process.

2.5. Step II: gap-filling procedures

Gap filling was undertaken as five successive operations (denoted steps II.1 to II.5) in order to account for the multiple structures of missing data and variables involved (Figure 3).

In step II.1, cubic spline interpolation was applied to Ta, RH and Pa to reconstruct single-point missing data. This operation was validated by simulation for a random sample from the synoptic series. A stochastic component, randomly drawn from a Gaussian distribution defined by the mean and standard deviation of the error on the validation sample, was added to each estimation to account for uncertainty in this interpolation.

Step II.2 focused on RH, which presented large sequences of missing data. A strong linear relationship was generally found between RH and Ta for a given day-of-year (DoY) and hour-of-day (HoD), consistently with findings by Guichard *et al.* (2009). RH was estimated at 2920 synoptic times with statistically significant

Table 3. Ancillary data sets from nearby stations. Measurement heights for the ARM and Wankama data sets were 2 m (except for U: 3 m) and 3 m, respectively. For these data sets, all SW_{down} values above clear-sky radiation, as defined by Allen et al. (1998), were set to clear-sky radiation. Websites to access data are specified in Appendix S3.

Data set	Source	Lon, Lat (°)	Distance from the Niamey airport station (km)	Period	Variables	Available data (%)[a]	Temporal resolution	References
Banizoumbou	Hapex-Sahel	2.651, 13.519	54	1991–1993	Ta, RH, SW_{down}	88	1 h	Goutorbe *et al.*, 1994
Agrhymet	Agrhymet	2.101, 13.496	7	1953–1979 2003–2009	Ta, RH	90 98	1 month 1 h	Boyer *et al.*, 2006
ARM	ARM	2.174, 13.477	1	2006	Ta, RH, U, Pa, q, SW_{down}, LW_{down}	97	30 min	ARM, 1993; ARM, 1994; Slingo *et al.*, 2006; Miller and Slingo, 2007
Wankama	AMMA-CATCH	2.630, 13.644	54	2005–2013	P, Ta, RH, q, SW_{down}, LW_{down}, U, Pa	100	30 min	Cappelaere *et al.*, 2009; Ramier *et al.*, 2009; Velluet *et al.*, 2014

[a]Across all variables during the period in which the data set was available.

Table 4. Methodological steps of NAD construction.

Steps	Variables concerned	Temporal resolution	Continuous series
I: Quality checking	P, Ta, RH, U, Pa	24 h, 12 h, 3 h, 5 min	No
II: Gap filling	P, Ta, RH, U, Pa	3 h, 5 min	Yes
II: Merging of data sets	P, Ta, RH, q, U, Pa	30 min	Yes
IV: Estimation of radiation	SW_{down}, LW_{down}	30 min	Yes
V: Estimation of surface responses	SW_{up}, LW_{up}, LE, H, G, Ts	30 min	Yes

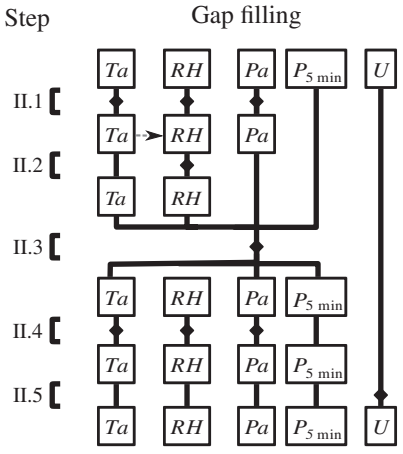

Figure 3. NAD construction methodology: description of the gap-filling operations (steps II.1–II.5) performed in step II. Boxes correspond to variables (symbols defined in Table 1), filled diamonds designate transformations performed at each step. Temporal resolution of variables at step II was 3 h, except for $P_{5\,min}$.

linear regression equations (p-value < 0.05 and $R^2 > 0.6$). Again, stochastic components randomly drawn from the Gaussian error distributions were added to each estimation to account for uncertainty.

In step II.3, remaining missing data for all variables except U were jointly estimated through a multivariable analysis gap-filling procedure. An analogue method, similar to that of Séguis *et al.* (2004), was devised to generate stochastically an ensemble of possible occurrences using all available information at different temporal resolutions (24 h, 12 h, 3 h, 5 min). For each day (denoted d) showing missing synoptic and/or precipitation values, data were selected from days, within a 30-DoY window centred on DoY(d) (DoY for day d) of the full data record, with characteristics 'similar' to those of day d. Similarity was defined by a decision tree based on timing and amplitude of variables for which data were available on day d. One among the 'similar' days was then randomly selected to fill up the incomplete day d. Hence, variables missing simultaneously were reconstructed with data from the same day, preserving inter-variable coherence. When the decision tree was unsuccessful (similarity criteria of the decision tree never met), a day was taken randomly within the whole 30-DoY window record (step II.4). Technical details can be found in Appendix S1.

Wind speed was not handled through the above operations because the criteria used were not relevant for this variable. No strong linkages could be established with other variables, so that U was reconstructed separately (step II.5). For each year with missing data, a different year was first randomly selected. Data from this year with the same DoY as the missing data were then used to fill in the gaps. As the selected year could itself contain missing data, the process was iterated until all gaps were filled. This

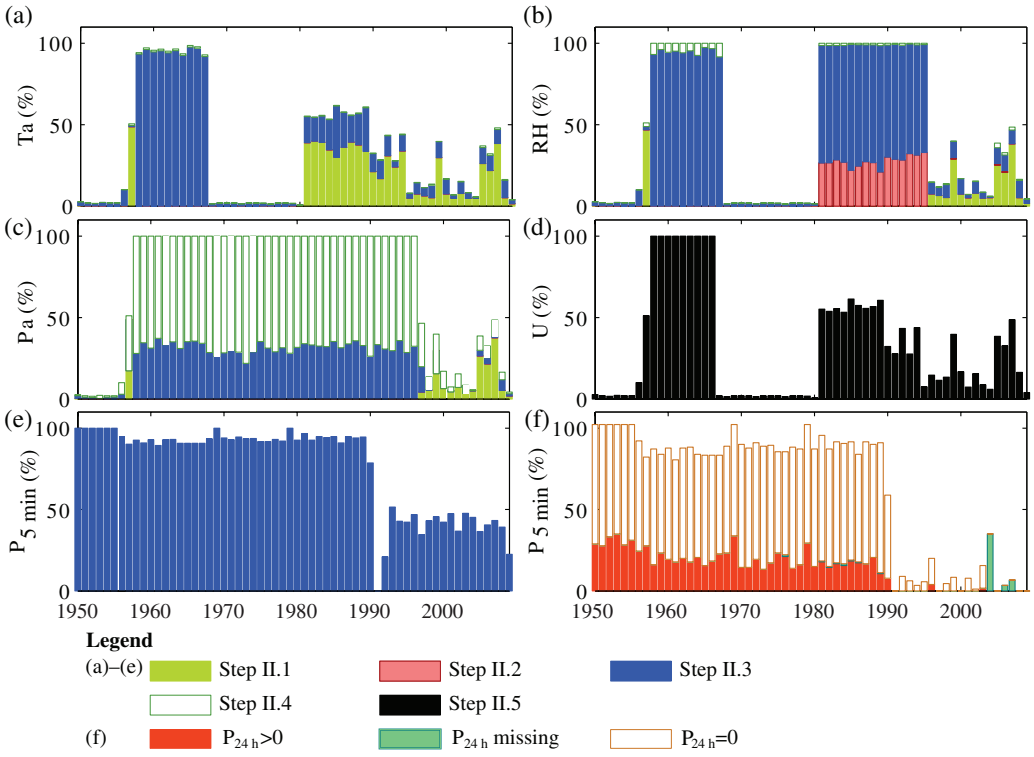

Figure 4. Data availability over time and operations performed for the reconstruction: (a)–(e) Yearly percentage of missing data per year for 5-min precipitation and 3-h meteorological variables. Colours indicate reconstruction operations in step II. (f) Availability of critical information to reconstitute $P_{5\,min}$ in the multivariate analogue method (step II.3). Percentages in (f) are relative to the May–October rainy season only. Please see variable definitions in Table 1.

was done to preserve as much as possible of the statistical properties of the variable, such as the auto-correlation over short timescales.

2.6. Step III: merging of synoptic and 5-min data

In step III, the two 3-h (Ta, RH, Pa, U) and 5-min data sets were merged into a single series at a 30-min time step. Synoptic data were disaggregated using cubic spline interpolation, a method validated against the Wankama high-resolution data set. As in step II, an additive stochastic component was randomly drawn from the Gaussian distribution fitted to the errors on the validation set. $P_{5\,min}$ was aggregated to $P_{30\,min}$.

2.7. Step IV: estimation of downwelling radiation

Methods described in the previous sections could not be used to estimate SW_{down} and LW_{down}, as these were not measured at Niamey airport station. Furthermore, existing general-purpose equations (Brutsaert, 1975; Hargreaves and Samani, 1982; Prata, 1996) only provide daily estimates and were found to underestimate wet season variability. Therefore, tailor-made artificial neural networks – capable of identifying complex non-linear relationships – were preferred, to derive downwelling radiation from available variables. Two neural networks, estimating SW_{down} or LW_{down} from extraterrestrial radiation R_{ext}, DoY, HoD, Ta and P, were trained with the 8-year Wankama data set. They were then successfully validated against the 1-year ARM data to verify transferability to the Niamey Airport location. To reflect training errors, an additive stochastic component for each HoD and DoY was drawn from the error distribution. Technical details are presented in Appendix S2.

2.8. Step V: application to estimation of land surface response variables (NAD-S)

The NAD-M series of meteorological variables, produced by steps I–IV, was finally applied to a physically based SVAT model to obtain estimates of land surface fluxes for two typical land cover types, fallow bush and millet crop. Description of these land cover types can be found in Boulain *et al.* (2009) and in Velluet *et al.* (2014).

The simple soil-plant-atmosphere transfer (SiSPAT) model (Braud *et al.*, 1995) was used to simulate the energy and water transfers in these two systems. It had previously been used successfully to simulate the water and energy cycles for these land cover types in the Sahel conditions (Braud *et al.*, 1997; Velluet *et al.*, 2014), and reliable calibration was available for these land cover types at the nearby Wankama observatory (Velluet, 2014; Velluet *et al.*, 2014). To limit computational time, a random subset of ten ensemble members from NAD-M was used for meteorological forcing of the model. For each land cover type, a mean seasonal cycle for leaf area was derived from the Wankama field data, and was applied with a phasing in time based on the rainfall pattern of each simulated year (growth was assumed to be initiated with the second >10 mm rainfall event). Dynamics of

vegetation rooting and height, as well as values for the model's ecophysiological and soil parameters, were taken from Velluet *et al.* (2014).

3. Characteristics of new NAD data series

This section highlights the main characteristics of the new NAD series, in terms of amount of reconstructed data (Section 3.1) and of the series' key properties, as to uncertainty, climatology, and relation to pre-existing data sets, both at short timescales (diurnal and seasonal, Section 3.2) and at large timescales (annual to decadal, Section 3.3). These properties are derived from the ten-member ensemble covering all NAD-M and NAD-S variables.

Note that detailed performance criteria for the different data reconstruction steps (steps II and IV) are analysed in Appendix A1. Altogether, they reflect upon the ensemble-described uncertainty distributions associated with each data entry in the data set.

3.1. Extent of reconstructed data

For $P_{5\,min}$, most missing data corresponded to days for which raw observations of $P_{24\,h}$ were nil, with only 13% occurring in days for which $P_{24\,h} > 0$ and 2.5% in days for which no precipitation data were available (Figure 4(f)).

Respectively, 34, 48, 70 and 32% of Ta, RH, Pa and U series' volumes were reconstructed (Figure 4(a)–(e)). Missing data for the original synoptic series were unevenly distributed in time, with essentially the following patterns: (1) most data were available for 1950–1957; (2) all variables were missing for 1958–1967; (3) most data, except Pa, were available for 1968–1979; (4) RH and Pa were entirely missing, whilst more than 60% of data were available for Ta and U, for 1980–1995; (5) less than 30% data were missing for all variables during 1996–2009.

For Ta, 11% of the series were reconstructed by single-point interpolation (step II.1). The multivariate analogue method (step II.3) reconstructed 22 and 37% of Ta and RH series, respectively. Additionnally, 4 and 6% of the RH series were reconstructed by spline interpolation (step II.1) and linear regression from observed Ta (step II.2), respectively. For Pa, 23% of the whole series were reconstructed with the multivariate analogue method, against 43% by the seasonal drawing of step II.4. Note however that the amplitude of Pa is rather small in this region (973–993 hPa for the Wankama series), with little influence on land surface processes.

Finally, the NAD-S land surface response subset is wholly synthetic, obtained by model transfer from the Wankama observatory.

3.2. Diurnal and annual cycles

When compared with the ARM field data set, and by contrast with ERA-Interim, the NAD-M series correctly reproduced the monthly mean diurnal cycles of all variables (Figure 5, illustrating three different months of 2006, in the dry and wet seasons). This is particularly obvious for precipitation and surface wind speed, for which the differences between ERA-Interim and ARM/NAD-M are very similar to those reported in previous studies (Nikulin *et al.*, 2012; Largeron *et al.*, 2015). For land surface variables, diurnal variations agree well all year round with the Wankama field observations (Velluet, 2014), as illustrated by Figure 5 for the millet cover.

Uncertainties due to the reconstruction methods are depicted at the sub-daily scale in Figure 6, which shows 24-h series for the ten ensemble members for 5 illustrative days, for which either all data were available (columns a and b) or for which availability gradually decreased (columns c–e). Uncertainty is generally lower during the dry season (columns a and b). Uncertainty logically increases with decreasing availability of data (left to right), but the general diurnal cycle is still distinguishable even when no data were available (Figure 6(e)). Figure 6 further illustrates the good agreement in diurnal cycle between NAD-M and ARM. In most cases, the uncertainty affecting meteorological variables at the sub-daily scale falls down at the daily scale (Figures 6 and 7(a) showing distributions of daily ensemble ranges). Even though a few days showed large uncertainties (outliers in Figure 7(a), essentially when no data were available), most daily values had low uncertainties (see, e.g. 75th percentiles to compare to ten ensemble member mean values in Figure 7(a)), a noticeable exception being wind speed U in the 1960s.

Furthermore, the composite annual cycles over 2006–2009 for both hydro-meteorological and surface flux variables were quite similar to those of the Wankama series for this overlapping period (Figure 8), although SW_{down}, q and H for millet are respectively higher, lower and higher for the Wankama series by $8.9\,W\,m^{-2}$, $1.7\,g\,kg^{-1}$ and $9.9\,W\,m^{-2}$. The composite annual cycle over 1950–2009 (Figure 8) further agree with comparable data for Central Sahel (Guichard *et al.*, 2015, not shown). Cycles for the different variables are imprinted by the basic dry/wet season pattern, with monomodal (e.g. q, LE) or bimodal (e.g. Ta) behaviours (see Ramier *et al.*, 2009; Guichard *et al.*, 2009 or Velluet *et al.*, 2014, for detailed analysis). Variability of SW_{down} increases markedly during the rainy season, in relation to cloud cover. LE, and consequently H, shows the largest variability throughout the rainy season due to the large temporal variability in precipitation.

3.3. Inter-annual and multi-decadal variability

3.3.1. NAD properties

Over the period 1950–2009, annual ensemble mean precipitation ranged from 293 to 979 mm (Figure 9(a), and Table 5), with a mean and standard deviation of 561 and 141 mm. Precipitation fluctuations were quite similar to those analysed by Séguis *et al.* (2004), reflecting in particular the severe regional droughts of the early 1970s and 1980s. All other meteorological and land cover-related variables, except Pa, also showed strong inter-annual fluctuations (Figure 9(b)–(l), thick black, green or blue lines

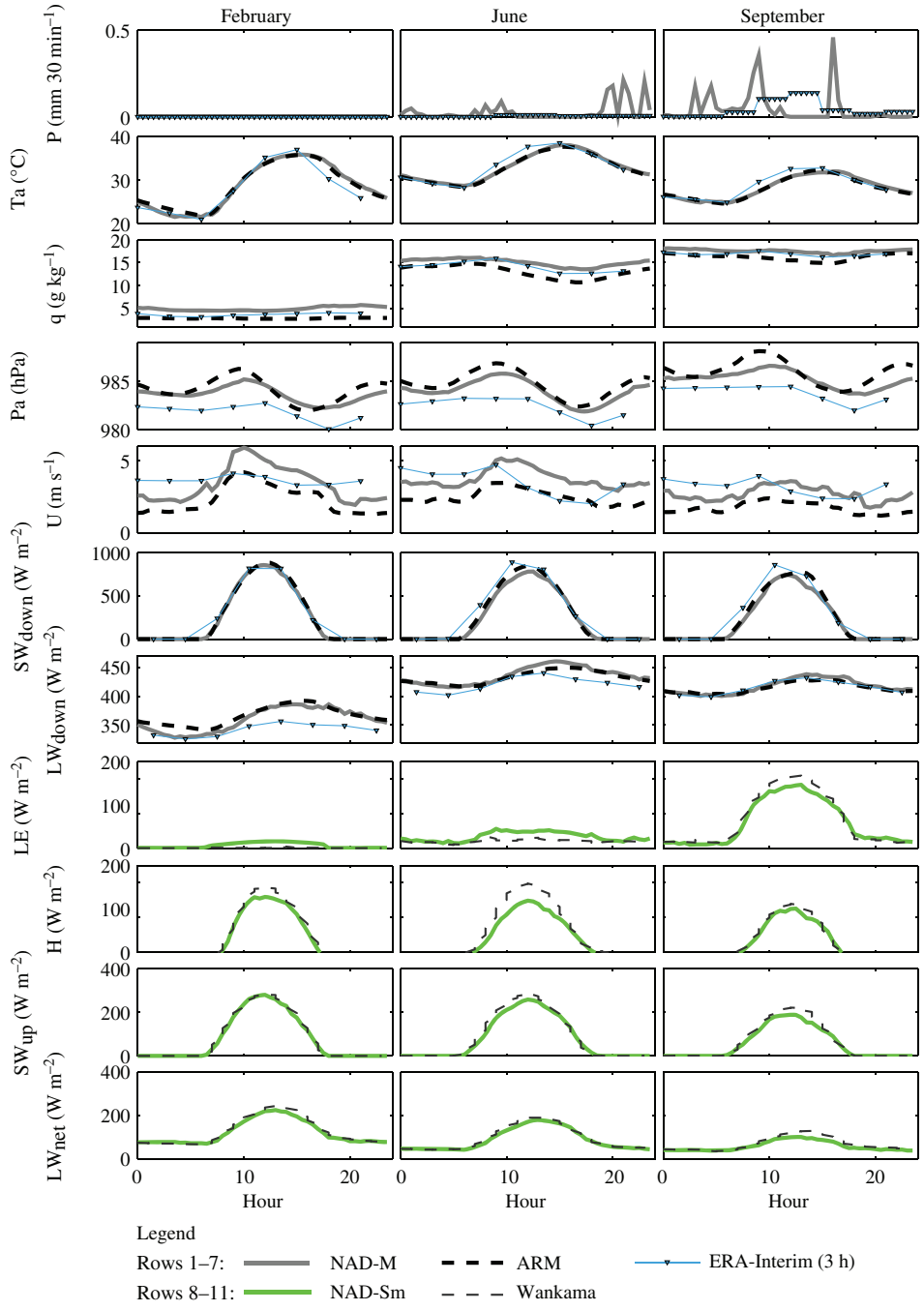

Figure 5. Diurnal cycles (30-min resolution): February, June and September 2006 monthly composites (left to right) for ARM, NAD-M, NAD-Sm (millet cover) and ERA-Interim data sets, for meteorological (P, q, Pa, U, SW_{down}, LW_{down}) and land surface variables (LE, H, SW_{up}, LW_{net}), Rows 1–7 and 8–11, respectively. For ERA-Interim, the $P_{3\ h}$ values were evenly distributed to display 30-min mean precipitation rates. Note that differences in U are also due to different measurement heights.

for NAD ensemble means) reflecting the large Sahelian climatic variability. In particular, the strong anomalies of Ta observed between 1969 and 1980 at Niamey are traced throughout West Africa, although they were distinct from larger scale fluctuations (Figure 10(a)). The 1969 and 1973 peaks are a record of the 1970s drought although the signal is more complex as they correspond to dry and rainy season anomalies, respectively. An increase by ∼1 °C in Ta (against an inter-annual standard deviation of 0.5 °C) was noted over the six-decade period (Table 5). Wind speed U is stronger during the period 1974–2009 than 1950–1974, with relatively low values during 1967–1973 (Figure 9(g)). The latter coincide with the high-temperature and low precipitation of this first regional drought period and could therefore be another feature of this very strong climatic anomaly. A similar pattern can be seen in recently published data for a station ∼1000 km east of Niamey (Hassane *et al.*, 2016), strengthening the significance of this observation. Annual LW_{down} was strongly correlated to Ta (correlation:

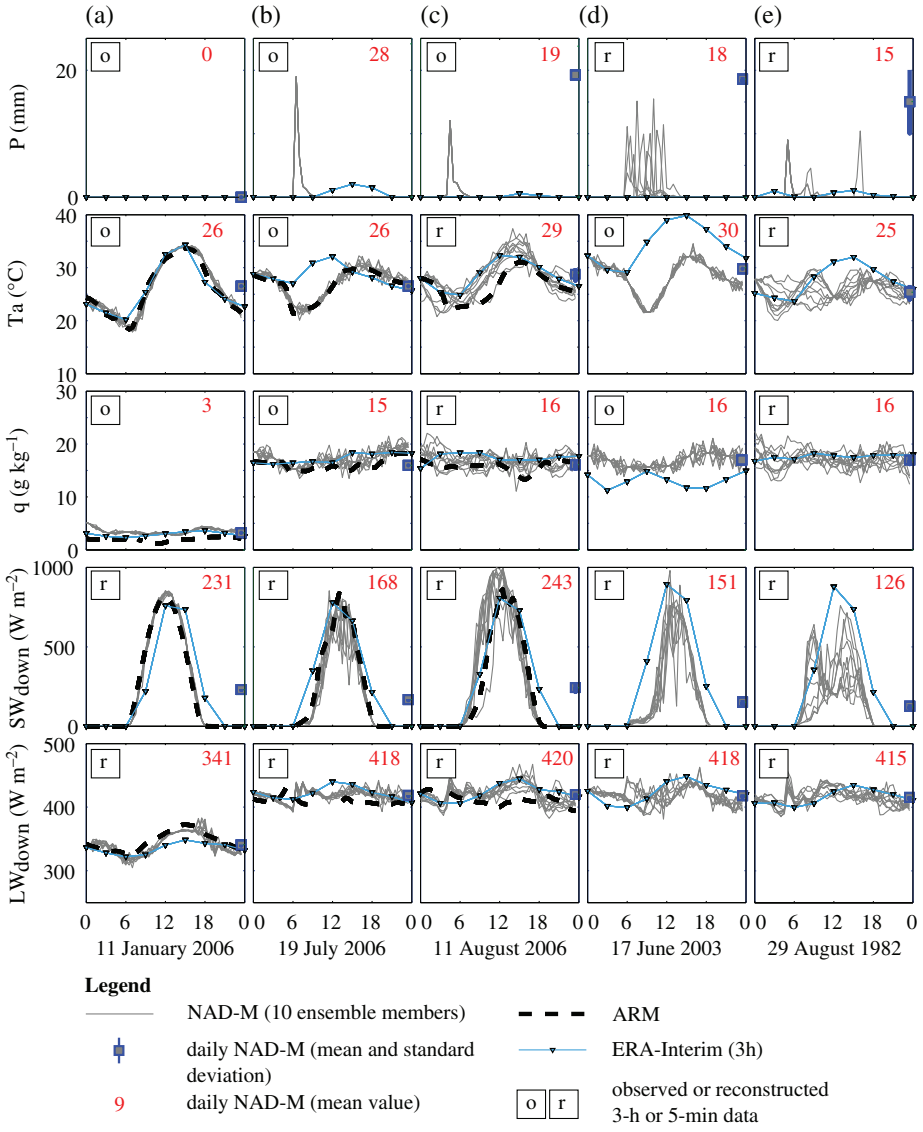

Figure 6. Diurnal cycles (30-min resolution) and mean daily values (24-h cumulated value for P and average for other variables) for $P_{30\ min}$, $P_{24\ h}$, Ta, q, SW_{down} and LW_{down} for selected days for which different types of data were available, illustrating the effects of data availability on the uncertainty of variable reconstruction at a sub-daily and daily scale. Available data for each column of graphs are, from left to right: (a) $P_{5\ min}$, 3-h climatic variables, for the dry season; (b) same, for the rainy season; (c) $P_{5\ min}$; (d) 3-h climatic data and $P_{24\ h}$; (e) no data available. ARM and ERA-Interim 3-h data are shown for comparison.

$\rho = 0.92$). By contrast, LW_{down} was only mildly related to P ($\rho = -0.31$), as was SW_{down} to Ta and P ($\rho = 0.24$ and -0.13). LE was highly correlated to P ($\rho = 0.71$ and $\rho = 0.81$ for millet and fallow bush, respectively) with lows during the 1970s and 1980s droughts. On the contrary, H was negatively correlated to P ($\rho = -0.65$ and $\rho = -0.73$, respectively) and LE ($\rho = -0.73$ and $\rho = -0.86$, respectively). SW_{up} (respectively, LW_{up}) was systematically higher (respectively, lower) for fallow bush compared with millet crop.

Uncertainty in the estimation of annual precipitation was low (1.7% ratio of median annual uncertainty to inter-annual ten-member ensemble mean P, Figure 7(b)). This was even more so for annual Ta and q, with the above ratio being 0.2 and 0.9%, respectively; Figures 7(b) and 9(b) and (c)). U and Pa (the latter not shown in Figure 9) were entirely reconstructed for the period 1958–1967, and additionally over 1975–1995 for Pa and 1980–1989 for U. As 24-h values were not available, the reconstruction procedure did not strongly constrain U during these periods (Figure 7(b)), but uncertainty remained globally acceptable (above ratio of 13.2%). The uncertainties in surface flux variables (Figure 9(h)–(l)) were directly linked to those of the meteorological variables. For example, uncertainties in U led to the highest uncertainties in the surface flux variables for H and LW_{up} through the partitioning of downwelling radiation. All in all, and except for U, annual-scale uncertainty linked to the gap-filling and estimation procedures was lower than inter-annual variability, lending confidence in the NAD-M subset. Resulting uncertainties were very low for mean decadal values (Table 5).

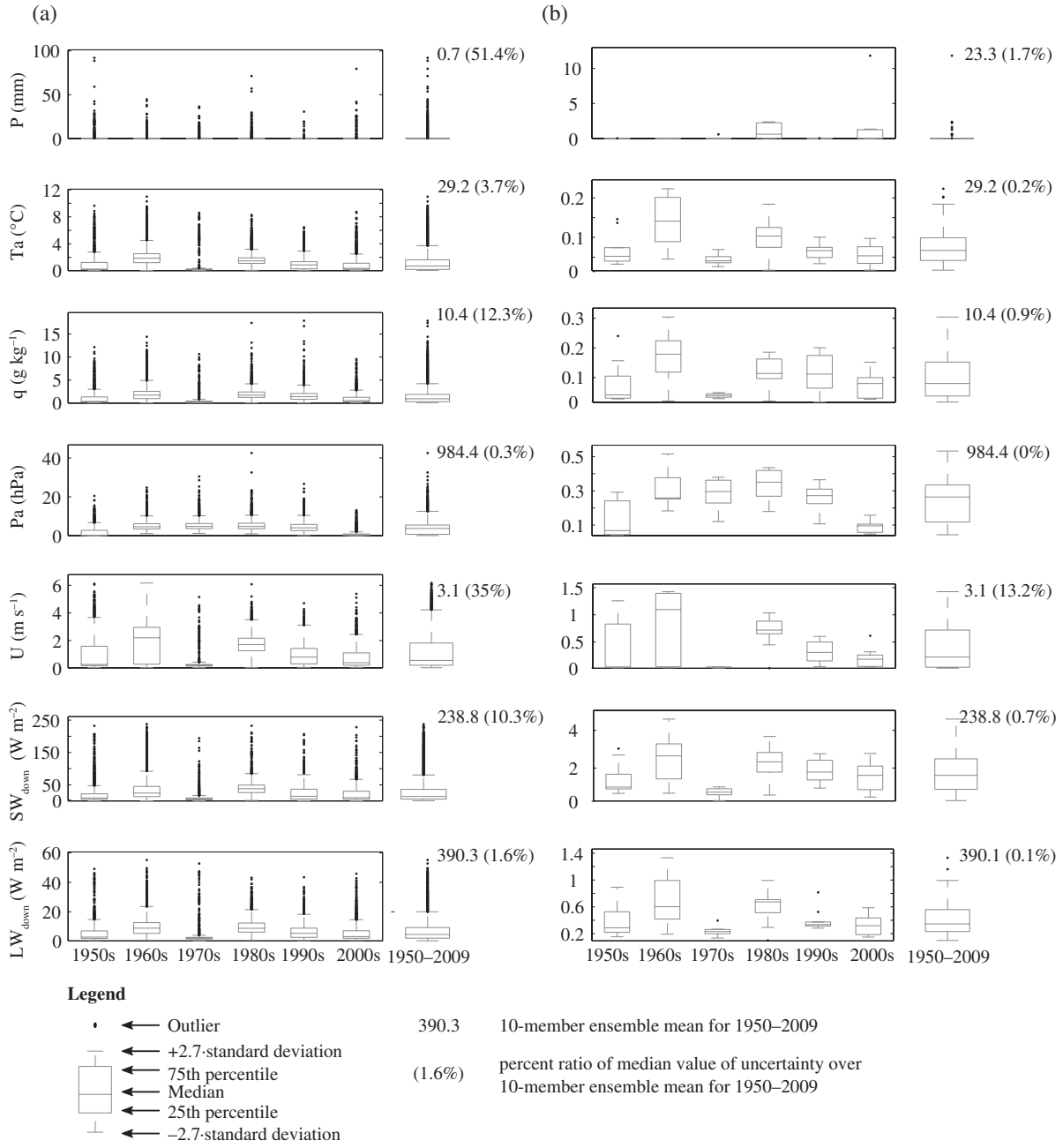

Figure 7. Boxplots of uncertainties for the NAD-M variables at the (a) daily and (b) annual scales, for each decade and the average for 1950–2009. Each uncertainty value is the range width between the minimum and maximum daily or annual value taken from the ten-member ensemble. The ten-member ensemble mean and the ratio of the median value of uncertainty over the ten-member ensemble mean for 1950–2009 (noted as a percentage) are specified.

3.3.2. Comparison of NAD-M with other data sets

Annual values of NAD-M were compared (Table 6 and Figure 9) with data sets from close-by stations (Agrhymet, ARM, Banizoumbou, Wankama), gridded data sets (CRU, GHCN-CAMS – hereafter referred to as GHCN, SRB) or meteorological re-analyses (ERA-40, ERA-Interim, NCEP2 and MERRA) – see Appendix A2 for gridded and re-analysis data sets specifics. The negative anti-correlation in P between NAD and Wankama (∼60 km apart; note however 8-year sample only) reflects the strong spatial variability in Sahelian precipitation. On longer timescales, annual precipitation from CRU (552 ± 115 mm) and NAD-M were positively correlated ($\rho = 0.81$) and consistent with observed multi-decadal fluctuations (Le Barbe *et al.*, 2002). By contrast, re-analyses data did not capture the 1950–2009 mean nor the decadal values of precipitation observed at Niamey airport station and characteristic of the region (Tables 5 and 6 and Figure 9(a)).

Annual Ta mean and variability were remarkably close for NAD-M and the longest gridded data sets (CRU, GHCN), supporting the ∼1 °C increase detected over the full period (Figure 9(b)). Annual values were slightly

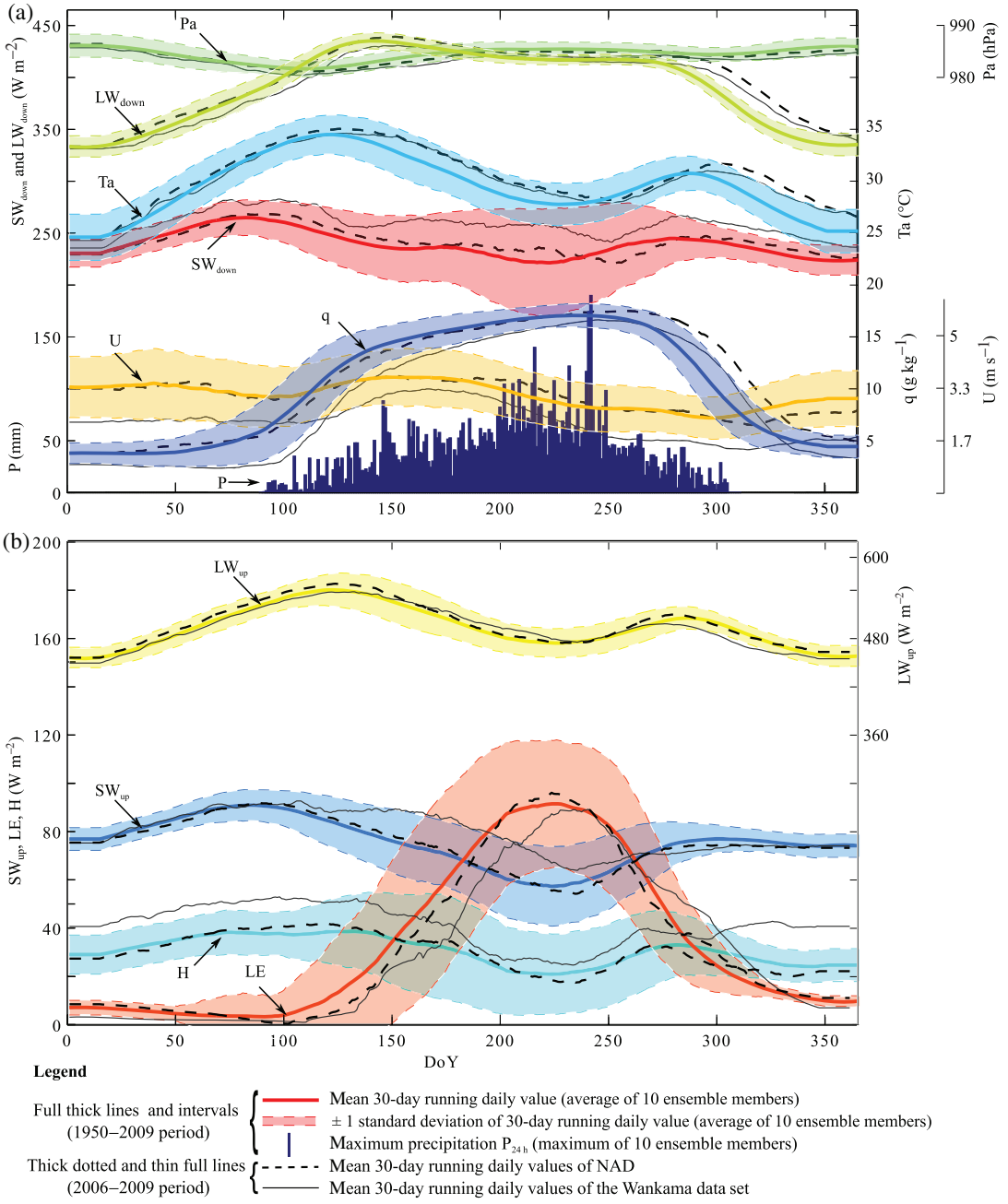

Figure 8. 1950–2009 composite annual cycle: (a) mean and standard deviation in 30-DOY running window of ten-member daily ensemble average for each NAD-M meteorological variable; full DOY range shown for ten ensemble members of precipitation $P_{24\,h}$, to highlight the maximum rainy season extent. (b) Same for energy response variables of NAD-Sm (millet land cover type). Mean 2006–2009 cycle at Wankama station superimposed for comparison with the mean 2006–2009 cycle for NAD-M and NAD-Sm. Note that differences in U between NAD and Wankama data sets can also be due to different measurement heights.

higher compared to GHCN but lower compared with the other data sets. It's noteworthy that ERA-40 does not capture the 1969–1980 temperature anomalies. NCEP2 was found to be much colder compared with all other long-term data sets (also found otherwise for the whole Sahel). Finally, correlation with Agrhymet was also high ($\rho = 0.74$), especially for the 1953–1979 period ($\rho = 0.88$).

q and RH were slightly higher in NAD-M compared with the Wankama and ARM series, with a mean annual difference of 2.06 g kg^{-1} between NAD-M and ARM (Table 6). This difference arose from the original RH data and could be due to either instrumental or environmental differences between stations (see Appendix S4). However, correlation with ERA-40 was high ($\rho \geq 0.80$) and inter-annual variability was well reproduced (Figure 9(c) and (d)).

LW_{down} was well correlated with the Wankama data ($\rho = 0.95$) and with NCEP2 ($\rho = 0.73$) and to a lesser degree with ERA-40, ERA-Interim and MERRA, but with lower inter-annual variability in NAD-M. Also, it was generally higher than the other long-term data sets while in very good agreement with the ARM 2006

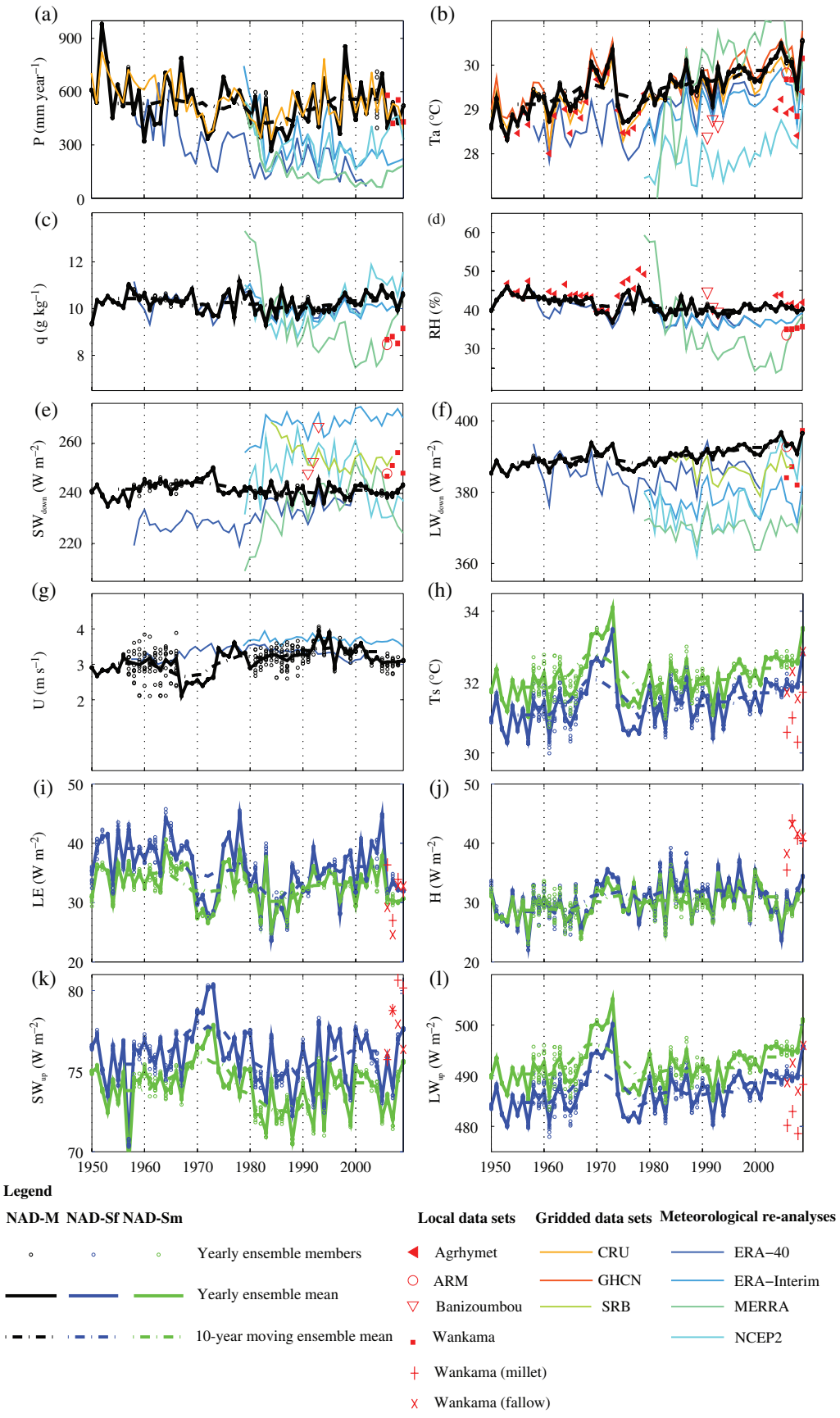

Figure 9. 1950–2009 diachronic analysis of yearly values for NAD-M meteorological variables ((a)–(g), variable name on y-axis), and for NAD-Sf and NAD-Sm energy response variables (h)–(l). All plots (a)–(l) show ten ensemble members, their mean and 10-year moving average, as well as available external values for local, gridded or re-analysis data sets. Pressure, displaying little inter-annual variability (Table 5), is not shown.

Table 5. NAD at annual to decadal scales. Centre columns: mean decadal values (bold) and standard deviation (italic) for ten ensemble members from 1950s to 2000s. Right columns: statistical characteristics (mean, standard deviation, maximum, minimum) of mean annual variables in NAD-M and NAD-S over 1950–2009. For NAD-S (bottom): grey, millet; white, fallow.

	Variable	Unit	Decade						Mean	Standard deviation	Maximum	Minimum
			1950s	1960s	1970s	1980s	1990s	2000s				
NAD-M	P	mm year^{-1}	**638.6** *0.1*	**657.3** *0.1*	**522.2** *0.5*	**458.0** *3.8*	**546.2** *0.0*	**542.4** *9.4*	561	141	979	293
	Ta	°C	**28.7** *0.0*	**29.0** *0.0*	**29.1** *0.0*	**29.1** *0.0*	**29.4** *0.0*	**29.8** *0.0*	29.2	0.5	30.3	28.2
	q	g kg^{-1}	**10.6** *0.0*	**10.6** *0.0*	**10.4** *0.0*	**10.2** *0.0*	**10.3** *0.0*	**10.6** *0.0*	10.4	0.4	11.4	9.5
	Pa	hPa	**984.5** *0.0*	**984.5** *0.0*	**984.4** *0.0*	**984.5** *0.0*	**984.5** *0.0*	**984.4** *0.0*	984.5	0.2	985.1	984.0
	U	m s^{-1}	**2.9** *0.1*	**2.9** *0.1*	**3.0** *0.0*	**3.2** *0.1*	**3.4** *0.0*	**3.2** *0.0*	3.1	0.3	3.9	2.1
	SW_{down}	W m^{-2}	**238.2** *0.1*	**241.5** *0.2*	**243.4** *0.1*	**234.0** *0.3*	**236.9** *0.2*	**238.9** *0.1*	238.8	4.8	249.8	225.2
	LW_{down}	W m^{-2}	**387.7** *0.0*	**388.6** *0.1*	**388.9** *0.0*	**390.1** *0.1*	**392.0** *0.0*	**393.4** *0.0*	390.1	2.8	396.5	384.2
NAD-S	SW_{up}	W m^{-2}	**73.7** *0.0*	**74.5** *0.1*	**75.5** *0.0*	**72.6** *0.1*	**73.5** *0.1*	**74.1** *0.0*	73.9	1.6	77.7	69.2
	SW_{up}	W m^{-2}	**75.3** *0.1*	**76.1** *0.1*	**77.6** *0.0*	**74.8** *0.1*	**75.5** *0.1*	**76.0** *0.1*	75.8	1.8	80.3	70.5
	LW_{up}	W m^{-2}	**489.8** *0.3*	**491.9** *0.3*	**493.6** *0.1*	**491.1** *0.3*	**491.5** *0.1*	**495.2** *0.1*	492.2	4.1	504.9	485.1
	LW_{up}	W m^{-2}	**484.1** *0.3*	**486.4** *0.5*	**488.3** *0.1*	**486.7** *0.3*	**486.9** *0.1*	**489.9** *0.1*	487.1	4.2	500.1	480.2
	LE	W m^{-2}	**34.1** *0.1*	**35.1** *0.2*	**32.0** *0.1*	**30.2** *0.1*	**33.4** *0.1*	**32.6** *0.1*	32.9	3.2	39.5	25.5
	LE	W m^{-2}	**38.5** *0.2*	**39.2** *0.2*	**34.8** *0.1*	**31.2** *0.2*	**34.9** *0.1*	**35.8** *0.2*	35.7	4.8	44.7	24.1
	H	W m^{-2}	**28.4** *0.3*	**28.5** *0.4*	**31.1** *0.1*	**30.3** *0.5*	**30.5** *0.1*	**30.2** *0.1*	29.8	2.5	35.0	24.1
	H	W m^{-2}	**28.5** *0.2*	**28.6** *0.3*	**31.8** *0.1*	**31.7** *0.5*	**31.8** *0.1*	**30.6** *0.1*	30.5	3.2	37.3	22.8
	Ts	°C	**31.8** *0.0*	**32.1** *0.1*	**32.4** *0.0*	**32.0** *0.1*	**32.1** *0.0*	**32.6** *0.0*	32.1	0.6	34.0	31.1
	Ts	°C	**31.0** *0.0*	**31.4** *0.1*	**31.7** *0.0*	**31.4** *0.1*	**31.4** *0.0*	**31.9** *0.0*	31.4	0.6	33.5	30.3

annual LW_{down} (Figure 9(f)). Correlations in SW_{down} between NAD-M and the other long-term data sets were poor over 1950–2009 (e.g. with ERA-40: $\rho = -0.16$), but improved after 1985 ($\rho = 0.73$ with ERA-40, mean difference of 4.8 W m^{-2}). Big discrepancies between the various re-analyses data for SW_{down} and LW_{down} suggest that these variables are difficult to estimate (Roehrig *et al.*, 2013). By contrast, our data set provides estimates of these radiative fluxes that are consistent with quality field data at the nearby sites. Finally, it is noteworthy that MERRA P, Ta and q were in disagreement with the gridded data, the re-analysis data and the current data set, suggesting that it does not properly capture the climatic conditions in Central Sahel.

Comparison of surface flux estimates was challenging as only the Wankama series (3-year overlap), showing an appropriate closure of the energy balance, was available. Climatological differences in forcing fluxes (P, q, SW_{down}) probably explains the observed inter-annual differences between estimates (Figure 9(h) and (l)) as the partitioning of SW_{down} into the components of the mean annual energy budgets, albeit absolute differences in H fluxes of ~10 W m^{-2}, were similar (Table 7).

4. Discussion

The originality of this study was to make use of complementary original data sets, consistent with each other and with overall infrequent missing data, to constitute a data set fit for modelling purposes. Their different characteristics led us to select multiple gap-filling methods that made best use of the wide variety of information available. These methods appeared to preserve the main features of the climatology of Central Sahel from the sub-daily to the decadal scale and allowed to estimate the uncertainty relative to the reconstructed variables. In particular, the analogue method as used by Séguis *et al.* (2004) was generalized to jointly estimate several hydro-meteorological variables, thus conserving inter-variable coherence. Neural networks provided estimations of SW_{down} and LW_{down} that reproduced well the typical

Table 6. Comparison with existing data sets: correlation (bold) and mean difference (italic) in annual values of the main meteorological variables between NAD-M and other data sets.

Variable	Gridded data sets			Meteorological re-analyses				Local data sets			
	CRU	GHCN	SRB	ERA-40	ERA-Interim	MERRA	NCEP2	Agrhymet	Banizoumbou	Wankama	ARM
P (mm year^{-1})	**0.81**	–	–	**0.31**	**−0.06**	**−0.16**	**−0.02**	–	–	**−0.95**	–
	8	–	–	*266*	*194*	*354*	*222*	–	–	*−4.4*	–
Ta (°C)	**0.88**	**0.91**	–	**0.71**	**0.86**	**0.61**	**0.69**	**0.74**	**−0.51**	**0.91**	–
	−0.03	*−0.19*	–	*0.49*	*0.43*	*0.12*	*1.60*	*0.36*	*0.84*	*0.30*	*0.11*
q (g kg^{-1})	–	–	–	**0.82**	**0.69**	**0.08**	**0.71**	–	–	**0.79**	–
	–	–	–	*0.11*	*0.21*	*0.86*	*0.12*	–	–	*1.60*	*2.06*
RH (%)	–	–	–	**0.80**	**0.63**	**0.33**	–	**0.79**	**0.85**	**0.11**	–
	–	–	–	*2.4*	*2.9*	*6.2*	–	*−1.8*	*−1.4*	*5.2*	*7.5*
U (m s^{-1})	–	–	–	**−0.17**	**0.23**	–	–	–	–	**−0.5**	–
	–	–	–	*−0.2*	*−0.4*	–	–	–	–	*0.8*	–
SW_{down} (W m^{-2})	–	–	**−0.14**	**−0.16**	**0.39**	**0.07**	**−0.13**	–	**0.89**	**−0.13**	–
	–	–	*−18*	*8*	*123*	*2*	*−10*	–	*−20*	*−10*	*−12*
LW_{down} (W m^{-2})	–	–	**0.37**	**0.54**	**0.50**	**0.39**	**0.73**	–	–	**0.95**	–
	–	–	*6*	*5*	*13*	*21*	*14*	–	–	*4*	*0*

Table 7. Mean annual energy budgets (W m^{-2}) for millet and fallow bush land cover types over 2006–2009, for the NAD and Wankama data sets.

Data set	SW_{down}	SW_{up}	LW_{net}	LE	H	G
NAD-Sm	242.7 (100%)	75.5 (31%)	103.8 (43%)	30.8 (13%)	31.1 (13%)	1.5 (∼0%)
Wankama	251.6 (100%)	77.4 (31%)	103.3 (41%)	29.8 (12%)	41.0 (16%)	0.1 (∼0%)
NAD-Sf	242.7 (100%)	77.7 (32%)	98.5 (41%)	32.6 (14%)	32.5 (13%)	1.4 (∼0%)
Wankama	248.6 (100%)	79.0 (32%)	97.7 (39%)	32.3 (13%)	40.1 (16%)	0.2 (∼0%)

annual and diurnal cycles. These networks, when properly trained, could offer an alternative to commonly used formulae (Brutsaert, 1975; Hargreaves and Samani, 1982; Prata, 1996). Note that the gap-filling methodology developed here could be easily applied to other synoptic stations where long-term data are available. More generally, the significance of trends in ensemble data sets, as the one constructed in this study, could be assessed by analysing each individual ensemble member separately, and applying a statistical test based on the percentage of members for which a given trend is detected.

Concerning estimated variables, precipitation and temperature were the most robust, with respect to complementary data sets. Trends in precipitation observed by Lebel and Ali (2009) for Central Sahel were satisfied. Temperatures were in good agreement with CRU and GHCN and showed a strong increase by ∼1 °C in mean annual temperature between the 1950s and 2000s, in accordance with another Sahelian site (Hombori, Mali; Guichard *et al*., 2015) and compared to the 0.85 °C global warming during 1880–2012. Furthermore, inter-annual variability and trend in Ta were in good agreement with mean regional values. All hydrological and land surface variables, although to a lesser degree for SW_{down}, q and H, showed satisfying diurnal and seasonal cycles compared with recent data from proximate sites (Guichard *et al.*, 2009 and Velluet *et al.*, 2014).

Some limitations to the methodology applied in this study appear. First, the multivariate analogue method is a delicate balance between the number and quality of similarity criteria used and the flexibility of these criteria to obtain reasonable pool sizes. Thus, some second-order conditions such as known non-stationarities over the period (essentially, the characteristics of rainstorm events in the 20–35 mm range, Lubès-Niel *et al*., 2001; sub-daily temperatures, Guichard *et al*., 2015) could not be accounted for. Second, the land surface flux components of the data set provide a long-term local reference, in accordance with proximate observed data (Velluet, 2014; Velluet *et al.*, 2014). However, they are modelled from a single SVAT model, compared with the NAD-M components that are based on observed data. Due to the lack of long-term observational data of these variables, these first estimates need to be confirmed, possibly using a multi-model intercomparison approach based on models adapted to local conditions, such as SiSPAT. A third limitation, inherent to the use of historical data, concerns potentially undetected errors within the raw data or changing station characteristics. The BEST metadata (Rohde *et al.*, 2013) only indicate a move of the station in 1950. Further verifications (displacements, change of sensors, etc.) are difficult to undertake due to the lack of metadata. The wind speed anomalies cannot be considered as inconsistent with the other variables, however wind speed data being particularly sensitive to measurement conditions, possible heterogeneity in original data cannot be entirely dismissed. Concerning the possibility of adjusting the series for spatial consistency, the comparison of Ta with

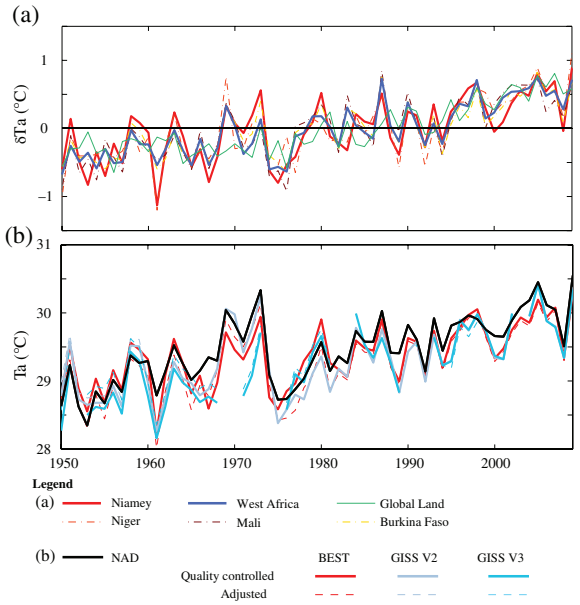

Figure 10. Annual air temperature (Ta) over 1950–2009: (a) comparison of Ta temporal anomaly in the BEST data set (δTa, yearly difference from period mean) over different domains, showing consistency across scales in West Africa compared to global land domain. (b) Comparison of NAD with BEST and GISS data sets, including 'quality controlled' and 'adjusted' series. Adjusted series take into account the consistency of a spatial network.

adjusted series that do take into account this consistency (GISS, Hansen *et al.*, 2010; BEST) shows that differences are smaller between the two versions from a given source (quality controlled versus adjusted) than between the different sources (Figure 10(b)). Fourth, although it has been shown that fluctuations of LW_{down} are driven by air temperature (Slingo *et al.*, 2009) and vapour-pressure (Culf and Gash, 1993; Stephens *et al.*, 2011), a humidity term was not used in its estimation as the neural networks were sensitive to inter-site variability of q. Future research should focus on improving the estimation of LW_{down} and SW_{down} and their long-term fluctuations. Finally, the fifth and main shortcoming of this data set is evidently that is it not spatially distributed, limiting modelling applications to local-scale analyses.

5. Conclusion

Important environmental changes have occurred in the Sahel region over the past 50 years, in a context of very high population growth and vulnerable rural societies. Robust modelling of the environmental systems would help to better understand these changes, but is impeded by data scarcity when the decadal timescale is considered. Serious for meteorological data, this problem is even more acute when it comes to land surface response variables for which no long-term, field-based series exist. As a first step towards alleviating this problem, we have built a 1950–2009 continuous, high-temporal resolution local data set, covering both groups of variables with the second one (NAD-S) being derived through model simulation from the former (NAD-M).

Despite the limitations discussed, the NAD series (1) offers a unique length and resolution, (2) provides a good representation at the diurnal to annual scales, (3) maintains inter-variable coherence, (4) reflects the uncertainty of the reconstruction methods for the meteorological data through an ensemblist approach, and (5) is representative of known inter-annual variability and trends for at least P and Ta. We believe that this data set is substantially more reliable than many commonly used data sets. Indeed, contrary to many gridded data sets, this local data set is based solely on observations and not on meteorological re-analyses that suffer from many deficiencies in the Sahel. Albeit being a point data set, it may represent in statistical terms a large Central Sahel region, thanks to the high degree of longitudinal stationarity in Sahelian climate and the length of the series.

This data set could serve as a high-quality baseline for climate change impact studies, in particular to evaluate historical Global Climate Model estimations, meteorological re-analyses and larger scale surface data sets (Sheffield *et al.*, 2006; Weedon *et al.*, 2011). As a continuous high-frequency data set, it can also be used in a variety of land surface, vegetation and hydrological modelling exercises (e.g. Leauthaud *et al.*, 2015 and Appendix S4 for guidelines). Public data distribution being an important issue for climate and environmental studies, especially in this region, the NAD data set will be made available through the AMMA-CATCH website (http://www.amma-catch.org/spip.php?article240).

Acknowledgements

The Niamey airport meteorological station is operated by the Direction de la Météorologie Nationale (DMN) of the Republic of Niger. Data were obtained from the DMN, the World Meteorological Organisation, the AMMA programme, the AMMA-CATCH observatory, the ARM Climate Research Facility of the US Department of Energy, Météo-France, AGRHYMET, and the SIEREM and Hapex-Sahel databases. Fruitful discussions with Julie Carreau on neural network methodology are gratefully acknowledged. This research was funded by the French National Research Agency through the ESCAPE project (ANR-10-CEPL-005).

Appendix

A1. Performances of estimation procedures

A1.1. Evaluation of deterministic methods

Spline interpolations and linear regressions of synoptic data

Only a small number of data points were estimated by spline interpolation in step II.1 (11% for Ta and <4% for RH and Pa). Nonetheless, results were verified by comparing simulated values to a randomly selected set of observed values from the original synoptic data sets.

Table A1. Mean, bias, root mean square error (RMSE) and Nash-Sutcliffe (NS) coefficient between observed and estimated (spline interpolation) values, calculated on validation subsets from the raw data at the Niamey airport station or at the Wankama station.

Variable	Data set	Step	Mean	Bias	RMSE	NS
Ta (°C)	Original synoptic series	Step II.1	29.1	−0.1	1.7	0.91
RH (%)	Original synoptic series	Step II.1	41	∼0	6	0.93
Pa (hPa)	Original synoptic series	Step II.1	984	∼0	1	0.82
Ta (°C)	Wankama	Step III	29.6	∼0	0.7	0.98
RH (%)	Wankama	Step III	35	∼0	2	0.99
Pa (hPa)	Wankama	Step III	983	∼0	∼0	0.96
U ($m\,s^{-1}$)	Wankama	Step III	2.2	∼0	1	0.80

Measured and simulated values showed good agreement with low bias and high Nash−Sutcliffe (NS) coefficients for all three variables (Table A1).

Concerning the gap filling of RH in step II.2, a total of 905−1114 data were used to estimate synoptic RH for given DoY and HoD by linear regression between Ta and RH. RH data for which the regression test performed with a p-value < 0.05 and $R^2 > 0.6$ were filled, corresponding to 6% of RH.

Spline interpolation in step III was validated on the Wankama data set, using the same procedure as in step II.1. Measured and simulated values showed good agreement with low biases and high NS coefficients for all variables (Table A1).

Estimation of downwelling radiation

Fourteen sets of input data were tested to estimate SW_{down} (see Appendix S2). All comprised extraterrestrial radiation R_{ext}, DoY and HoD, and differed by the presence or absence of Ta, q and P. The artificial neural network (ANN) constructed at the Wankama site that used Ta and P and presented a low RMSE (RMSE = 78 $W\,m^{-2}$ for a mean of 493 $W\,m^{-2}$ for the validation population) was selected. It was less efficient during the rainy season (RMSE = 89 $W\,m^{-2}$) although SW_{down} during rainy events was better simulated (RMSE = 83 $W\,m^{-2}$). This ANN for SW_{down} simulated the output variable with a high NS coefficient (NS > 0.9) for both the Wankama and ARM data sets, although estimations were slightly biased negatively in both cases (Table A2). The mean bias at Wankama was substracted for the estimation of SW_{down} in NAD.

Input variables for LW_{down} were selected from fourteen sets, in a similar way to SW_{down} (see Appendix S2). For the final selected ANN, also using Ta and P, RMSE was quite low (RMSE = 15 $W\,m^{-2}$ for a mean of 392 $W\,m^{-2}$ on the validation population). The ANN was more efficient during the rainy season (RMSE = 12 $W\,m^{-2}$) and during rainy events (RMSE = 12 $W\,m^{-2}$). This ANN also simulated LW_{down} well at the ARM site (NS =0.87) (Table A2).

Table A2. Mean ($W\,m^{-2}$), bias ($W\,m^{-2}$), RMSE ($W\,m^{-2}$) and Nash−Sutcliffe NS (−) coefficients for 30 min SW_{down} and LW_{down} estimated by ANNs in step IV, for the ARM and Wankama series.

Variable	Data sets	Mean value	Bias	RMSE	NS
SW_{down}	Wankama	491	−7	78	0.93
SW_{down}	ARM	497	−17	79	0.93
LW_{down}	Wankama	392	0	15	0.87
LW_{down}	ARM	389	−2	14	0.87

A1.2. Quality of the analogue and other stochastic methods

Relevance of criteria for the analogue method

A whole set of criteria were used in the analogue method to constrain reconstructed data by observed data and to retain coherence between variables at the sub-daily scale. First, pool classes were circumscribed by observed Ta_{mean}, RH_{mean} and $P_{24\,h}$, so that the reconstructed ensemble member 3-h or 5-min Ta, RH and P variables preserved these daily features of the observed data. Second, based on the analysis of the ratio of synoptic temperature Ta over the potential maximal synoptic temperature (noted Ta/Ta_{cs}), the analogue method also retained when possible the co-variation of the hydro-meteorological variables throughout a rainfall event (Appendix S1 for technical details). Third, in the rare case where precipitation $P_{5\,min}$ was reconstructed in the absence of $P_{24\,h}$, rainfall occurrence was again constrained by synoptic temperature. Indeed, the daily minimum ratio of synoptic temperature Ta over the potential maximal synoptic temperature (Ta/Ta_{cs}) was also found to be significantly different between rainy days and non rainy days (0.73 ± 0.08 and 0.81 ± 0.06, respectively), during the rainy season (t-test, 5% significance level): a rainfall event was hence reconstructed when Ta/Ta_{cs} <0.8. Finally, in the last case where daily values of synoptic data were unavailable, pools were formed with data from a 30-DoY window so that the seasonal cycle at least was preserved.

Random selection and recursive gap filling

In the case where the analogue method was not retained (representing only <1% for Ta and RH, and 43% for Pa. Note however the low inter-annual variability of Pa, Table 5), data were randomly selected from the observed data available within a 30-DoY window. Pa, which mainly presented seasonal variability, was hence well reconstructed. Similarly, all missing data for wind speed were reconstructed by recursive gap filling. In both cases, these methods, although they do not constrain the reconstructed data tightly, at least enabled an estimation of the uncertainty ranges in the absence of reliable predictive data.

A2. Specifications of the global and re-analysis data sets

Characteristics of the gridded data sets are provided in Table A3.

Table A3. Specifications for the global or re-analysis data sets. 'NCEP2' refers to the NCEP/DOE AMIP-II Reanalysis (Reanalysis-2). Websites are specified in Appendix S3.

Data set	Period	Grid (lon–lat)	Variables extracted	Temporal resolution	Number of cells used	References
MERRA	1979–2010	0.67°–0.5°	Ta, LW_{down}, Pa, q, RH, SW_{down}, U, P	Annual	2	Rienecker *et al.*, 2011
GHCN	1950–2009	0.5°–0.5°	Ta	Annual, monthly	4	Fan and van den Dool, 2008
CRU TS3.10	1950–2009	0.5°–0.5°	Ta, P	Annual, monthly	4	Mitchell and Jones, 2005; Harris *et al.*, 2014
SRB 3.0 & 3.1	1984–2007	1°–1°	SW_{down}, LW_{down}	Annual	9	–
ERA-40	1958–2001	1°–1°	Ta, RH, q, LW_{down}, SW_{down}, P	Annual[a]	4	Uppala *et al.*, 2005
ERA-Interim	1979–2010	1°–1°	Ta, RH, LW_{down}, SW_{down}, P	Annual[a], 3-Hour[b]	4	Dee *et al.*, 2011
NCEP2	1979–2013	1.9°–1.9°	Ta, q, LW_{down}, SW_{down}, P	Annual	4	Kanamitsu *et al.*, 2002

[a]Annual data from the 6-h analysis values, except SW_{down} and LW_{down}. [b]The 3-h forecast data set included Ta (2 m), LW_{down}, SW_{down}, RH, q, U (10 m), P. Pa (6 h resolution) was used to calculate q at a 3-h resolution.

Table A4. List of corrections/adjustments applied in step I.

Context	Data sets or variable	Concerned data volume (%)[a]	Comments
Incoherent meteorological data	Ta	0.03	Ta max. and min. thresholds set to 45 and 9 °C, respectively
	RH	$<10^{-4}$	RH > 100%: RH set to 100%
	U	20	Inconsistent unit in SYN1 from 1967 to 1980 (rel. to SYN2): SYN1 values corrected (from kt to m s^{-1}) over the period
	U	0.02	U max. threshold set to 25 m s^{-1}
	Pa	0.1	Pa max. and min. thresholds set to 1000 hPa and 970 hPa, respectively
	DLY1	0.2	Abnormal rain event changed to missing data
	DLY2	4	Ta_{mean} from DLY2 incoherent with SYN2 or SYN3: Ta_{mean} not used in analysis
	DLY2	28	RH_{mean} from DLY2 incoherent with SYN2 or SYN3: RH_{mean} not used in analysis
Incoherent rain data	$P_{5\,min}$	0.4	$P_{24\,h} > 0$ & $\Sigma P_{5\,min} = 0$: $P_{5\,min}$ set as missing data
	DLY1	0.15	Rainy day from $P_{24\,h}$ found one day after $\Sigma P_{5\,min}$: $P_{24\,h}$ modified to fit with $P_{5\,min}$
	DLY1	0.03	Rainy day from $P_{24\,h}$ found one day before $\Sigma P_{5\,min}$: $P_{24\,h}$ modified to fit with $P_{5\,min}$
Discontinued rain event data	$P_{5\,min}$	38	Missing $P_{5\,min}$ values within days for which $P_{24\,h}$ and $\Sigma P_{5\,min}$ were concordant, were set to 0

[a]Total amount of data per variable (n): DLY1 and DLY2: $n = 23337$; Ta, RH, U and Pa: $n = 187.10^3$; $P_{5\,min}$: $n = 6.7.10^6$.

A3. Corrections applied in step I

During assemblage of the different series into series of identical temporal resolution, when concomitant data from different series were discordant (e.g. different values at the same time for two series), the most coherent data (e.g. correct rainfall pattern) from the longest series (case of FVE1) and coming from the same source (case of SYN1 and DLY1) were kept. All corrections applied in step I are listed in Table A4.

Supporting information

The following supporting information is available as part of the online article:

Appendix S1. Description of the multivariate analogue method.

Appendix S2. Training procedure of the artificial neural networks.

Appendix S3. Websites to access the data used in this study.

Appendix S4. Guidelines for the use of NAD.
Appendix S5. Choice of input data for the neural networks.

References

Allen, R.G., Pereira, L.S., Raes, D., Smith, M., 1998. Crop evapotranspiration – guidelines for computing crop water requirements. Irrigation and Drainage Paper 56. FAO, Rome, 300: D05109.

Balme M, Vischel T, Lebel T, Peugeot C, Galle S. 2006. Assessing the water balance in the Sahel: impact of small scale rainfall variability on runoff: Part 1: rainfall variability analysis. *J. Hydrol.* **331**: 336–348, doi: 10.1016/j.jhydrol.2006.05.020.

Boulain N, Cappelaere B, Ramier D, Issoufou HBA, Halilou O, Seghieri J, Guillemin F, Oï M, Gignoux J, Timouk F. 2009. Towards an understanding of coupled physical and biological processes in the cultivated Sahel – 2. Vegetation and carbon dynamics. *J. Hydrol.* **375**: 190–203, doi: 10.1016/j.jhydrol.2008.11.045.

Boyer JF, Dieulin C, Rouche N, Cres A, Servat E, Paturel JE, Mahe G. 2006. *Sierem: An Environmental Information System for Water Resources*. IAHS-AISH Publication, 308: 19–25.

Braud I, Dantas-Antonino AC, Vauclin M, Thony JL, Ruelle P. 1995. A simple soil-plant-atmosphere transfer model (SiSPAT) development and field verification. *J. Hydrol.* **166**: 213–250, doi: 10.1016/0022-1694(94)05085-C.

Braud I, Bessemoulin P, Monteny B, Sicot M, Vandervaere JP, Vauclin M. 1997. Unidimensional modelling of a fallow savannah during the HAPEX-Sahel experiment using the SiSPAT model. *J. Hydrol.* **188**: 912–945, doi: 10.1016/S0022-1694(96)03177-0.

Brutsaert W. 1975. On a derivable formula for long-wave radiation from clear skies. *Water Resour. Res.* **11**: 742–744, doi: 10.1029/WR011i005p00742.

Cappelaere B, Descroix L, Lebel T, Boulain N, Ramier D, Laurent J-P, Favreau G, Boubkraoui S, Boucher M, Bouzou Moussa I, Chaffard V, Hiernaux P, Issoufou HBA, Le Breton E, Mamadou I, Nazoumou Y, Oi M, Ottlé C, Quantin G. 2009. The AMMA-CATCH experiment in the cultivated Sahelian area of south-west Niger – investigating water cycle response to a fluctuating climate and changing environment. *J. Hydrol.* **375**: 34–51, doi: 10.1016/j.jhydrol.2009.06.021.

Chimani B, Matulla C, Böhm R, Hofstätter M. 2013. A new high resolution absolute temperature grid for the Greater Alpine Region back to 1780. *Int. J. Climatol.* **33**: 2129–2141, doi: 10.1002/joc.3574.

Culf A, Gash J. 1993. Longwave radiation from clear skies in Niger – a comparison of observations with simple formulas. *J. Appl. Meteorol.* **32**: 539–547, doi: 10.1175/1520-0450(1993)032<0539:LRFCSI>2.0.CO;2.

Dardel C, Kergoat L, Hiernaux P, Mougin E, Grippa M, Tucker CJ. 2014. Re-greening Sahel: 30 years of remote sensing data and field observations (Mali, Niger). *Remote Sens. Environ.* **140**: 350–364, doi: 10.1016/j.rse.2013.09.011.

Dee DP, Uppala SM, Simmons AJ, Berrisford P, Poli P, Kobayashi S, Andrae U, Balmaseda MA, Balsamo G, Bauer P, Bechtold P, Beljaars ACM, van de Berg L, Bidlot J, Bormann N, Delsol C, Dragani R, Fuentes M, Geer AJ, Haimberger L, Healy SB, Hersbach H, Hólm EV, Isaksen L, Kållberg P, Köhler M, Matricardi M, McNally AP, Monge-Sanz BM, Morcrette J-J, Park B-K, Peubey C, de Rosnay P, Tavolato C, Thépaut J-N, Vitart F. 2011. The ERA-Interim reanalysis: configuration and performance of the data assimilation system. *Q. J. R. Meteorol. Soc.* **137**: 553–597, doi: 10.1002/qj.828.

Falge E, Baldocchi D, Olson R, Anthoni P, Aubinet M, Bernhofer C, Burba G, Ceulemans R, Clement R, Dolman H, Granier A, Gross P, Grünwald T, Hollinger D, Jensen N-O, Katul G, Keronen P, Kowalski A, Ta Lai C, Law BE, Meyers T, Moncrieff J, Moors E, William Munger J, Pilegaard K, Rannik Ü, Rebmann C, Suyker A, Tenhunen J, Tu K, Verma S, Vesala T, Wilson K, Wofsy S. 2001. Gap filling strategies for long term energy flux data sets. *Agric. For. Meteorol.* **107**: 71–77, doi: 10.1016/S0168-1923(00)00235-5.

Fan Y, van den Dool H. 2008. A global monthly land surface air temperature analysis for 1948-present. *J. Geophys. Res.-Atmos.* **113**: D01103, doi: 10.1029/2007JD008470.

Favreau G, Cappelaere B, Massuel S, Leblanc M, Boucher M, Boulain N, Leduc C. 2009. Land clearing, climate variability, and water resources increase in semiarid southwest Niger: a review. *Water Resour. Res.* **45**: W00A16, doi: 10.1029/2007WR006785.

Gosset M, Viarre J, Quantin G, Alcoba M. 2013. Evaluation of several rainfall products used for hydrological applications over West Africa using two high-resolution gauge networks. *Q. J. R. Meteorol. Soc.* **139**: 923–940, doi: 10.1002/qj.2130.

Goutorbe J-P, Lebel T, Tinga A, Bessemoulin P, Brouwer J, Dolman AJ, Engman ET, Gash JHC, Hoepffner M, Kabat P, Kerr YH, Monteny B, Prince S, Said F, Sellers P, Wallace JS. 1994. HAPEX-Sahel: a large-scale study of land-atmosphere interactions in the semi-arid tropics. *Ann. Geophys.* **12**: 53–64, doi: 10.1007/s00585-994-0053-0.

Guichard F, Kergoat L, Mougin E, Timouk F, Baup F, Hiernaux P, Lavenu F. 2009. Surface thermodynamics and radiative budget in the Sahelian Gourma: seasonal and diurnal cycles. *J. Hydrol.* **375**: 161–177, doi: 10.1016/j.jhydrol.2008.09.007.

Guichard F, Kergoat L, Hourdin F, Leauthaud C, Barbier J, Mougin E, Diarra B. 2015. *Le réchauffement climatique observé depuis 1950 au Sahel*. Evolutions Récentes et Futures Du Climat En Afrique de l'Ouest: Evidences, Incertitudes et Perceptions, IRD, Paris, France.

Hansen J, Ruedy R, Sato M, Lo K. 2010. Global surface temperature change. *Rev. Geophys.* **48**: RG4004, doi: 10.1029/2010RG000345.

Hargreaves GH, Samani ZA. 1982. Estimating potential evapotranspiration. *J. Irrig. Drain. Div.* **108**: 225–230.

Harris IPDJ, Jones PD, Osborn TJ, Lister DH. 2014. Updated high-resolution grids of monthly climatic observations – the CRU TS3.10 dataset. *Int. J. Climatol.* **34**: 623–642, doi: 10.1002/joc.3711.

Hassane B, Durand A, Garba Z, Dieppois B, Sebag D, Rajot J-L, Diedhiou A, Ngounou Ngatcha B, Traore A. 2016. Can daily meteorological measurement of near-surface wind detect climate changes in the Sahel (SE Niger, 1950–1992)? *J. Arid Environ.* **124**: 91–101, doi: 10.1016/j.jaridenv.2015.07.014.

Herrera S, Gutiérrez JM, Ancell R, Pons MR, Frías MD, Fernández J. 2012. Development and analysis of a 50-year high-resolution daily gridded precipitation dataset over Spain (Spain02). *Int. J. Climatol.* **32**: 74–85, doi: 10.1002/joc.2256.

Hiernaux P, Ayantunde A, Kalilou A, Mougin E, Gerard B, Baup F, Grippa M, Djaby B. 2009a. Trends in productivity of crops, fallow and rangelands in Southwest Niger: impact of land use, management and variable rainfall. *J. Hydrol.* **375**: 65–77, doi: 10.1016/j.jhydrol.2009.01.032.

Hiernaux P, Mougin E, Diarra L, Soumaguel N, Lavenu F, Tracol Y, Diawara M. 2009b. Sahelian rangeland response to changes in rainfall over two decades in the Gourma region, Mali. *J. Hydrol.* **375**: 114–127, doi: 10.1016/j.jhydrol.2008.11.005.

Hulme M. 1992. Rainfall changes in Africa: 1931–1960 to 1961–1990. *Int. J. Climatol.* **12**: 685–699, doi: 10.1002/joc.3370120703.

Hulme M. 2001. Climatic perspectives on Sahelian desiccation: 1973–1998. *Glob. Environ. Change* **11**: 19–29, doi: 10.1016/S0959-3780(00)00042-X.

Ibrahim M, Favreau G, Scanlon BR, Seidel JL, Le Coz M, Demarty J, Cappelaere B. 2014. Long-term increase in diffuse groundwater recharge following expansion of rainfed cultivation in the Sahel, West Africa. *Hydrogeol. J.* **22**: 1293–1305, doi: 10.1007/s10040-014-1143-z.

Kahan DS, Xue Y, Allen SJ. 2006. The impact of vegetation and soil parameters in simulations of surface energy and water balance in the semi-arid Sahel: a case study using SEBEX and HAPEX-Sahel data. *J. Hydrol.* **320**: 238–259, doi: 10.1016/j.jhydrol.2005.07.011.

Kanamitsu M, Ebisuzaki W, Woollen J, Yang S-K, Hnilo JJ, Fiorino M, Potter GL. 2002. NCEP–DOE AMIP-II reanalysis (R-2). *Bull. Am. Meteorol. Soc.* **83**: 1631–1643, doi: 10.1175/BAMS-83-11-1631.

Klok EJ, Klein Tank AMG. 2009. Updated and extended European dataset of daily climate observations. *Int. J. Climatol.* **29**: 1182–1191, doi: 10.1002/joc.1779.

Largeron Y, Guichard F, Bouniol D, Couvreux F, Kergoat L, Marticorena B. 2015. Can we use surface wind fields from meteorological reanalyses for Sahelian dust emission simulations? *Geophys. Res. Lett.* **42**: 2490–2499, doi: 10.1002/2014GL062938.

Le Barbe L, Lebel T, Tapsoba D. 2002. Rainfall variability in West Africa during the years 1950-90. *J. Clim.* **15**: 187–202, doi: 10.1175/1520-0442(2002)015<0187:RVIWAD>2.0.CO;2.

Leauthaud C, Demarty J, Cappelaere B, Grippa M, Kergoat L, Velluet C, Guichard F, Mougin E, Chelbi S, Sultan B. 2015. Revisiting historical climatic signals to better explore the future: prospects of water cycle changes in Central Sahel. In *Proceedings of the International Association of Hydrological Sciences*, Prague, Czech Republic, 1–7 pp. doi: 10.5194/piahs-92-1-2015

Lebel T, Ali A. 2009. Recent trends in the Central and Western Sahel rainfall regime (1990-2007). *J. Hydrol.* **375**: 52–64, doi: 10.1016/j.jhydrol.2008.11.030.

Lebel T, Cappelaere B, Galle S, Hanan N, Kergoat L, Levis S, Vieux B, Descroix L, Gosset M, Mougin E, Peugeot C, Seguis L. 2009.

AMMA-CATCH studies in the Sahelian region of West-Africa: an overview. *J. Hydrol.* **375**: 3–13, doi: 10.1016/j.jhydrol.2009.03.020.

Leblanc MJ, Favreau G, Massuel S, Tweed SO, Loireau M, Cappelaere B. 2008. Land clearance and hydrological change in the Sahel: SW Niger. *Glob. Planet. Change* **61**: 135–150, doi: 10.1016/j.gloplacha.2007.08.011.

Lubès-Niel H, Séguis L, Sabatier R. 2001. Étude de stationnarité des caractéristiques des événements pluvieux de la station de Niamey sur la période 1956–1998. *C. R. Acad. Sci.* **333**: 645–650, doi: 10.1016/S1251-8050(01)01690-1.

Mahé G, Olivry J-C. 1999. Assessment of freshwater yields to the ocean along the intertropical Atlantic coast of Africa (1951–1989). *C. R. Acad. Sci.* **328**: 621–626, doi: 10.1016/S1251-8050(99)80159-1.

Massuel S, Cappelaere B, Favreau G, Leduc C, Lebel T, Vischel T. 2011. Integrated surface water–groundwater modelling in the context of increasing water reserves of a regional Sahelian aquifer. *Hydrol. Sci. J.* **56**: 1242–1264, doi: 10.1080/02626667.2011.609171.

Meynadier R, Bock O, Gervois S, Guichard F, Redelsperger J-L, Agustí-Panareda A, Beljaars A. 2010. West African Monsoon water cycle: 2. Assessment of numerical weather prediction water budgets. *J. Geophys. Res.-Atmos.* **115**: D19107, doi: 10.1029/2010JD013919.

Miller MA, Slingo A. 2007. The ARM mobile facility and its first international deployment: measuring radiative flux divergence in West Africa. *Bull. Am. Meteorol. Soc.* **88**: 1229–1244, doi: 10.1175/BAMS-88-8-1229.

Mitchell TD, Jones PD. 2005. An improved method of constructing a database of monthly climate observations and associated high-resolution grids. *Int. J. Climatol.* **25**: 693–712, doi: 10.1002/joc.1181.

Moffat AM, Papale D, Reichstein M, Hollinger DY, Richardson AD, Barr AG, Beckstein C, Braswell BH, Churkina G, Desai AR, Falge E, Gove JH, Heimann M, Hui D, Jarvis AJ, Kattge J, Noormets A, Stauch VJ. 2007. Comprehensive comparison of gap-filling techniques for eddy covariance net carbon fluxes. *Agric. For. Meteorol.* **147**: 209–232, doi: 10.1016/j.agrformet.2007.08.011.

Moorcroft PR. 2003. Recent advances in ecosystem-atmosphere interactions: an ecological perspective. *Proc. R. Soc. Lond. B: Biol. Sci.* **270**: 1215–1227, doi: 10.1098/rspb.2002.2251.

Nicholson SE. 2001. Climatic and environmental change in Africa during the last two centuries. *Clim. Res.* **17**: 123–144.

Nicholson SE, Some B, McCollum J, Nelkin E, Klotter D, Berte Y, Diallo BM, Gaye I, Kpabeba G, Ndiaye O, Noukpozounkou JN, Tanu MM, Thiam A, Toure AA, Traore AK. 2003. Validation of TRMM and other rainfall estimates with a high-density gauge dataset for West Africa. Part II: validation of TRMM rainfall products. *J. Appl. Meteorol.* **42**: 1355–1368, doi: 10.1175/1520-0450(2003)042<1355:VOTAOR>2.0.CO;2.

Nikulin G, Jones C, Giorgi F, Asrar G, Büchner M, Cerezo-Mota R, Christensen OB, Déqué M, Fernandez J, Hänsler A, van Meijgaard E, Samuelsson P, Sylla MB, Sushama L. 2012. Precipitation climatology in an ensemble of CORDEX-Africa regional climate simulations. *J. Clim.* **25**: 6057–6078, doi: 10.1175/JCLI-D-11-00375.1.

Panthou G, Vischel T, Lebel T. 2014. Recent trends in the regime of extreme rainfall in the Central Sahel. *Int. J. Climatol.* **34**: 3998–4006, doi: 10.1002/joc.3984.

Prata AJ. 1996. A new long-wave formula for estimating downward clear-sky radiation at the surface. *Q. J. R. Meteorol. Soc.* **122**: 1127–1151, doi: 10.1002/qj.49712253306.

Ramier D, Boulain N, Cappelaere B, Timouk F, Rabanit M, Lloyd CR, Boubkraoui S, Métayer F, Descroix L, Wawrzyniak V. 2009. Towards an understanding of coupled physical and biological processes in the cultivated Sahel – 1. Energy and water. *J. Hydrol.* **375**: 204–216, doi: 10.1016/j.jhydrol.2008.12.002.

Rienecker MM, Suarez MJ, Gelaro R, Todling R, Bacmeister J, Liu E, Bosilovich MG, Schubert SD, Takacs L, Kim G-K, Bloom S, Chen J, Collins D, Conaty A, da Silva A, Gu W, Joiner J, Koster RD, Lucchesi R, Molod A, Owens T, Pawson S, Pegion P, Redder CR, Reichle R, Robertson FR, Ruddick AG, Sienkiewicz M, Woollen J. 2011. MERRA: NASA's modern-era retrospective analysis for research and applications. *J. Clim.* **24**: 3624–3648, doi: 10.1175/JCLI-D-11-00015.1.

Roehrig R, Bouniol D, Guichard F, Hourdin F, Redelsperger J-L. 2013. The present and future of the West African monsoon: a process-oriented assessment of CMIP5 simulations along the AMMA transect. *J. Clim.* **26**: 6471–6505, doi: 10.1175/JCLI-D-12-00505.1.

Rohde R, Muller R, Jacobsen R, Perlmutter S, Rosenfeld A, Wurtele J, Curry J, Wickham C, Mosher S. 2013. Berkeley Earth Temperature Averaging Process. *Geoinform. Geostat.: An Overview* **1**: 2, doi: 10.4172/2327-4581.1000103.

Saux-Picart S, Ottlé C, Decharme B, André C, Zribi M, Perrier A, Coudert B, Boulain N, Cappelaere B, Descroix L, Ramier D. 2009. Water and energy budgets simulation over the AMMA-Niger super-site spatially constrained with remote sensing data. *J. Hydrol.* **375**: 287–295, doi: 10.1016/j.jhydrol.2008.12.023.

Schwalm CR, Williams CA, Schaefer K, Anderson R, Arain MA, Baker I, Barr A, Black TA, Chen G, Chen JM, Ciais P, Davis KJ, Desai A, Dietze M, Dragoni D, Fischer ML, Flanagan LB, Grant R, Gu L, Hollinger D, Izaurralde RC, Kucharik C, Lafleur P, Law BE, Li L, Li Z, Liu S, Lokupitiya E, Luo Y, Ma S, Margolis H, Matamala R, McCaughey H, Monson RK, Oechel WC, Peng C, Poulter B, Price DT, Riciutto DM, Riley W, Sahoo AK, Sprintsin M, Sun J, Tian H, Tonitto C, Verbeeck H, Verma SB. 2010. A model-data intercomparison of CO2 exchange across North America: results from the North American carbon program site synthesis. *J. Geophys. Res.* **115**: G00H05, doi: 10.1029/2009JG001229.

Séguis L, Cappelaere B, Milési G, Peugeot C, Massuel S, Favreau G. 2004. Simulated impacts of climate change and land-clearing on runoff from a small Sahelian catchment. *Hydrol. Processes* **18**: 3401–3413, doi: 10.1002/hyp.1503.

Sheffield J, Goteti G, Wood EF. 2006. Development of a 50-year high-resolution global dataset of meteorological forcings for land surface modeling. *J. Clim.* **19**: 3088–3111, doi: 10.1175/JCLI3790.1.

Slingo A, Ackerman TP, Allan RP, Kassianov EI, McFarlane SA, Robinson GJ, Barnard JC, Miller MA, Harries JE, Russell JE, Dewitte S. 2006. Observations of the impact of a major Saharan dust storm on the atmospheric radiation balance. *Geophys. Res. Lett.* **33**: L24817, doi: 10.1029/2006GL027869.

Slingo A, White HE, Bharmal NA, Robinson GJ. 2009. Overview of observations from the RADAGAST experiment in Niamey, Niger: 2. Radiative fluxes and divergences. *J. Geophys. Res.-Atmos.* **114**: D00E04, doi: 10.1029/2008JD010497.

Stephens GL, Wild M, Stackhouse PW, L'Ecuyer T, Kato S, Henderson DS. 2011. The global character of the flux of downward longwave radiation. *J. Clim.* **25**: 2329–2340, doi: 10.1175/JCLI-D-11-00262.1.

Uppala SM, KÅllberg PW, Simmons AJ, Andrae U, Bechtold VDC, Fiorino M, Gibson JK, Haseler J, Hernandez A, Kelly GA, Li X, Onogi K, Saarinen S, Sokka N, Allan RP, Andersson E, Arpe K, Balmaseda MA, Beljaars ACM, Berg LVD, Bidlot J, Bormann N, Caires S, Chevallier F, Dethof A, Dragosavac M, Fisher M, Fuentes M, Hagemann S, Hólm E, Hoskins BJ, Isaksen L, Janssen PEM, Jenne R, Mcnally AP, Mahfouf J-F, Morcrette J-J, Rayner NA, Saunders RW, Simon P, Sterl A, Trenberth KE, Untch A, Vasiljevic D, Viterbo P, Woollen J. 2005. The ERA-40 re-analysis. *Q. J. R. Meteorol. Soc.* **131**: 2961–3012, doi: 10.1256/qj.04.176.

Velluet C. 2014. *Modélisation et analyse pluriannuelles du fonctionnement hydrologique et énergétique de deux écosystèmes dominants au Sahel agropastoral (Sud-Ouest Niger)*. PhD thesis, Université Montpellier II – Sciences et Techniques du Languedoc.

Velluet C, Demarty J, Cappelaere B, Braud I, Issoufou HB-A, Boulain N, Ramier D, Mainassara I, Charvet G, Boucher M, Chazarin J-P, Oï M, Yahou H, Maidaji B, Arpin-Pont F, Benarrosh N, Mahamane A, Nazoumou Y, Favreau G, Seghieri J. 2014. Building a field- and model-based climatology of local water and energy cycles in the cultivated Sahel – annual budgets and seasonality. *Hydrol. Earth Syst. Sci.* **18**: 5001–5024, doi: 10.5194/hess-18-5001-2014.

Weedon GP, Gomes S, Viterbo P, Shuttleworth WJ, Blyth E, Österle H, Adam JC, Bellouin N, Boucher O, Best M. 2011. Creation of the WATCH forcing data and its use to assess global and regional reference crop evaporation over land during the twentieth century. *J. Hydrometeorol.* **12**: 823–848, doi: 10.1175/2011JHM1369.1.

Xue Y, De Sales F, Vasic R, Mechoso CR, Arakawa A, Prince S. 2010. Global and seasonal assessment of interactions between climate and vegetation biophysical processes: a GCM study with different land-vegetation representations. *J. Clim.* **23**: 1411–1433, doi: 10.1175/2009JCLI3054.1.

